AZURE: An *R*-matrix code for nuclear astrophysics

R. E. Azuma,[1,2] E. Uberseder,[2,*] E. C. Simpson,[2,3] C. R. Brune,[4] H. Costantini,[2,5] R. J. de Boer,[2] J. Görres,[2] M. Heil,[6] P. J. LeBlanc,[2] C. Ugalde,[2,†] and M. Wiescher[2]

[1]*Department of Physics, University of Toronto, Toronto, Ontario M5S 1A7, Canada*
[2]*University of Notre Dame, Department of Physics, Notre Dame, Indiana 46556, USA*
[3]*Department of Physics, Faculty of Engineering and Physical Sciences, University of Surrey, Guildford, Surrey GU2 7XH, United Kingdom*
[4]*Department of Physics and Astronomy, Ohio University, Ohio 45701, USA*
[5]*Istituto Nazionale Fisica Nucleare (INFN), Genova, Italy*
[6]*GSI Darmstadt, Planckstr. 1, 64291 Darmstadt, Germany*

(Received 11 January 2010; published 26 April 2010)

The paper describes a multilevel, multichannel *R*-matrix code, AZURE, for applications in nuclear astrophysics. The code allows simultaneous analysis and extrapolation of low-energy particle scattering, capture, and reaction cross sections of relevance to stellar hydrogen, helium, and carbon burning. The paper presents a summary of *R*-matrix theory, code description, and a number of applications to demonstrate the applicability and versatility of AZURE.

DOI: 10.1103/PhysRevC.81.045805 PACS number(s): 26.20.Cd, 25.40.Lw, 24.10.−i

I. INTRODUCTION

Stellar nucleosynthesis during the hydrogen, helium, and carbon burning phases of stellar evolution is characterized by radiative capture and nuclear fusion reactions of light particles. The reaction rates of these processes determine not only nucleosynthesis but also the energy production and time scale for these three consecutive stellar burning phases. The reaction rates $N_A\langle\sigma v\rangle$ at the characteristic stellar temperatures T are determined by the low-energy cross section $\sigma(E)$ of the respective nuclear reaction processes

$$N_A\langle\sigma v\rangle = \left(\frac{8}{\pi\mu}\right)^{1/2}\frac{N_A}{(kT)^{3/2}}\int_0^\infty \sigma(E)E\exp\left(-\frac{E}{kT}\right)dE, \tag{1}$$

where μ is the reduced mass, k is the Boltzmann constant, T is the temperature, and $\sigma(E)$ is the energy E dependent cross section.

The reaction cross sections $\sigma(E)$ of radiative capture and reaction processes on light nuclei are typically characterized by resonant and nonresonant reaction components. Extraordinary effort has been spent over the last decades to experimentally study and map the cross sections of critical reactions in stellar hydrogen, helium, and carbon burning. However, in the typical energy range of stellar burning, the cross sections are exceedingly low and in most cases cannot be measured directly with available techniques. Present reaction data in the stellar energy range are therefore mostly based on extrapolations of existing higher energy measurements [1]. A wide variety of theoretical tools have been introduced to reduce the associated uncertainties, starting from the concept of the S factor $S(E)$ to correct in first approximation for the effect of Coulomb repulsion for a straightforward extrapolation of the data [2]. The S factor for a reaction between two charged nuclei with atomic numbers Z_1 and Z_2 is given by

$$S(E) = \sigma(E)E\exp(2\pi\eta), \tag{2}$$

where $\eta = Z_1Z_2e^2/(\hbar v_0)$ is the Sommerfeld parameter, $v_0 = \sqrt{2E/\mu}$ the relative velocity of the interacting nuclei, and μ the reduced mass.

Traditionally, the extrapolation of low-energy radiative capture or reaction data for low-level-density compound systems utilized the single-level Breit-Wigner formula for resonance data [3], complemented by potential model based direct capture calculations [4–7] for nonresonant reaction components. On the other hand, reaction data on high-level-density compound systems were traditionally extrapolated on the basis of statistical Hauser-Feshbach theories [2,8]. The range of applicability depends critically on the level density in the compound nucleus as well as the typical widths of the resonance levels, which decrease rapidly with increasing charge Z [9]. This phenomenological approach is, in many cases, insufficient, since it often neglects more complex low-energy reaction mechanisms and contributions that are not directly reflected in the available higher energy data.

The introduction of *R*-matrix theory [10–12] allows for more reliable interpretation of the observed experimental data, since it makes it possible to accurately account for interference effects between multiple resonant and nonresonant contributions. While the classical *R*-matrix approach was limited to the treatment of resonant reactions in low-level-density systems [13], considerable effort was made to implement also nonresonant reaction mechanisms into the framework of *R*-matrix theory to describe more reliably the interplay between resonant and nonresonant reaction components [14]. The versatility of this approach was successfully demonstrated by the interpretation and extrapolation of the low-energy data of the $^{14}N(p,\gamma)^{15}O$ reaction [15], which determines nucleosynthesis, time scale, and energy production in the CNO cycles [16]. *R* matrix has emerged as a powerful tool for the

*Ethan.Uberseder.1@nd.edu
†Present address: Argonne National Laboratory, Argonne, Illinois 60439, USA.

analysis of stellar reaction rates, but in most cases R-matrix applications have been limited to a multilevel single-reaction approach that cannot consider additional data on scattering and other open reaction channels. This is a disadvantage in cases where interference effects or subthreshold contributions are more constrained by other reaction or scattering channels than that of astrophysical interest.

The multilevel, multichannel R-matrix code AZURE has been developed and optimized for the analysis and extrapolation of low-energy charged-particle reaction data of relevance to stellar nucleosynthesis processes. This paper will introduce the code AZURE and will demonstrate the applicability and versatility of the code for a number of reaction examples of relevance to stellar hydrogen burning.

In the following section, a short summary of R-matrix theory is given in the context of the AZURE development. This is followed by sections summarizing the parameter transformation theories of Barker [17] and Brune [18], and providing a short description of the code structure for the potential user. The following sections present three examples of the analysis of published low-energy reaction data. These examples include scattering data and capture reaction data dominated by resonant and/or nonresonant reaction contributions. Specifically, this consists of critical examples for our present interpretation of the CNO cycle [19,20] through a description of radiative capture data from $^{12}C(p,\gamma)^{13}N$, $^{14}N(p,\gamma)^{15}O$, and $^{16}O(p,\gamma)^{17}F$. The present study is based on the use of published, generally accessible reaction data and focuses on demonstrating the versatility of the multichannel R-matrix code techniques. The implications for resonance parameters and low-energy extrapolation of the associated cross sections will be presented and discussed within the limits of the available experimental data used for this study.

II. *R*-MATRIX THEORY

The basic assumption of the R-matrix approach is that the particle configuration space can be separated into two distinct regions: an internal region where the total wave function can be expanded into a complete set of eigenstates, and an external region where the possible combinations of coupled particle pairs, or channels, exist [21]. The interactions within the internal region are determined by the complicated many-body nuclear physics. The external region is assumed to contain only the Coulomb interaction between the particles and thus has a completely analytical solution depending only upon energy, masses, charges, and the intrinsic and relative angular momenta. Further development of R-matrix theory is then based on the assertion that the wave functions of the internal and external regions, and their derivatives, must match at the boundary surface.

A. Mathematical formalism

The fundamentals of the R-matrix formalism were reviewed in the encyclopedic publication of Lane and Thomas [21], and the notation of this reference has been retained unless otherwise noted. Additionally, the mathematical details of the theory have been well summarized by Vogt [22]. These publications extensively explain the basis of R-matrix theory, and therefore only a few key points will be outlined here.

1. From R-matrix to cross section

The wave functions at the surface defining the boundary between the internal and external regions of the compound nucleus can be expanded in terms of channels, where each channel is designated by a specific particle pair with a defined angular momentum coupling. In the notation of Ref. [21], channels are represented as $c = \alpha s l$, where s is the channel spin, l is the relative angular momentum of the interacting particles, and α identifies the interacting particle pair. In the following equations, c will be used when all indices α, s, and l should be considered as a group. If one of these indices is treated explicitly from the rest, for example, in a summation, the expanded notation will be used. In general, the dependencies of various quantities on the total spin J will be suppressed unless it plays an important role.

At the boundary surface, the radial part of the external channel wave function takes the form

$$\phi_c = \left(\frac{1}{v_c}\right)^{\frac{1}{2}} (y_c I_c + x_c O_c), \tag{3}$$

where I_c and O_c denote the incoming and outgoing wave functions which can be determined from the Coulomb wave functions F_c and G_c. The quantities y_c and x_c are the incoming and outgoing wave amplitudes, respectively, and v_c is the relative channel velocity. The collision matrix $\mathbf{U}$ is defined by the relation

$$x_c = -\sum_{c'} U_{cc'} y_{c'}, \tag{4}$$

and mediates the transformation from a set of incoming particle channels to outgoing particle channels. Substitution of Eq. (4) into Eq. (3) gives the external radial wave function in terms of the incoming wave amplitudes:

$$\phi_c = \left(\frac{1}{v_c}\right)^{\frac{1}{2}} \left(y_c I_c - \sum_{c'} U_{cc'} y_{c'} O_c\right). \tag{5}$$

A similar relation can be derived for the radial component of an internal channel wave function evaluated at the channel surface. This expression is given by

$$\phi_c = \left(\frac{m_c a_c}{\hbar^2}\right)^{\frac{1}{2}} \sum_{c'} R_{cc'} \left(\frac{\hbar^2}{m_{c'} a_{c'}}\right)^{\frac{1}{2}} [\rho_{c'} \phi'_{c'} - B_{c'} \phi_{c'}], \tag{6}$$

where m_c is the reduced mass, a_c is the channel radius, $\rho_c = k_\alpha a_c$, k_α is the wave number, and the prime denotes the derivative with respect to $k_\alpha r$. The B_c represent the boundary conditions in R-matrix theory or, more specifically, the logarithmic derivatives of an eigenstate wave function evaluated at the channel surface. This equation also introduces the R matrix which represents all the internal information concerning the structure of the compound system. Explicitly, the R matrix is defined as

$$R_{cc'} = \sum_{\lambda} \frac{\gamma_{\lambda c} \gamma_{\lambda c'}}{E_\lambda - E}, \tag{7a}$$

with

$$\gamma_{\lambda c} = \left(\frac{\hbar^2}{2m_c a_c}\right)^{\frac{1}{2}} \int dS X^*_\lambda \psi_c. \tag{7b}$$

The eigenstate wave function X_λ appears in the second equation as an overlap integral with the surface channel wave function ψ_c. The reduced width amplitude $\gamma_{\lambda c}$ is then a measure of the contribution of the level λ to the wave function of a channel c. The eigenenergy is denoted above as E_λ. In the present approach, the level energy and reduced width amplitudes are treated as parameters to be determined by experimental data.

When the logarithmic derivatives of the radial wave functions for the internal and external regions are matched at the channel surface, the subsequent expression can be solved for the collision matrix. In matrix form, this yields

$$\mathbf{U} = \boldsymbol{\rho}^{\frac{1}{2}}\mathbf{O}^{-1}(\mathbf{1} - \mathbf{RL_0})^{-1}(\mathbf{1} - \mathbf{RL_0^*})\mathbf{I}\boldsymbol{\rho}^{-\frac{1}{2}}. \tag{8}$$

With the exception of $\mathbf{R}$, all of the matrices in Eq. (8) are diagonal. The matrices $\boldsymbol{\rho}$, $\mathbf{I}$, $\mathbf{O}$, and $\mathbf{B}$ are defined to have diagonal elements ρ_c, I_c, O_c, and B_c, respectively. The matrix $\mathbf{L_0}$ is given by $\boldsymbol{\rho}\mathbf{O}'\mathbf{O}^{-1} - \mathbf{B}$. With the definition of two new diagonal matrices $\boldsymbol{\mathcal{B}} = \boldsymbol{\rho}\mathbf{I}^{-1}\mathbf{O}^{-1}$ and $\boldsymbol{\Omega} = \mathbf{I}^{\frac{1}{2}}\mathbf{O}^{-\frac{1}{2}}$, the collision matrix may be written in terms of a new matrix $\mathbf{W}$ with the relation $\mathbf{U} = \boldsymbol{\Omega}\mathbf{W}\boldsymbol{\Omega}$, where

$$\begin{aligned}\mathbf{W} &= \boldsymbol{\mathcal{B}}^{\frac{1}{2}}(\mathbf{1} - \mathbf{RL_0})^{-1}(\mathbf{1} - \mathbf{RL_0^*})\boldsymbol{\mathcal{B}}^{-\frac{1}{2}} \\ &= \mathbf{1} + \boldsymbol{\mathcal{B}}^{\frac{1}{2}}(\mathbf{1} - \mathbf{RL_0})^{-1}\mathbf{R}\boldsymbol{\mathcal{B}}^{\frac{1}{2}}\mathbf{w}.\end{aligned} \tag{9}$$

The final diagonal matrix in the above equation, $\mathbf{w}$, is the Wronskian of the functions O_c and I_c evaluated at the boundary surface. For positive energy channels, the elements of the diagonal matrices $\boldsymbol{\mathcal{B}}$ and $\mathbf{w}$ are

$$\mathcal{B}_{cc'} = P_c\delta_{cc'} \quad \text{and} \quad w_{cc'} = 2i\delta_{cc'}, \tag{10}$$

where P_c is the penetrability for channel c. The use of the $\mathbf{W}$ matrix is strictly a convenience, as it serves only to simplify the calculation of the collision matrix. The collision matrix can be related to the transition matrix $\mathbf{T}$ via

$$T_{cc'} = e^{2i\omega_c}\delta_{cc'} - U_{cc'}, \tag{11}$$

where ω_c represents the Coulomb phase shift.

It should be noted that there is *one* R matrix and thus *one* collision matrix for each grouping of like J^π levels. The respective channels that can populate a given R-matrix are restricted by conservation of both angular momentum and parity. For the calculation of cross sections, the dependence of $\mathbf{U}$ and $\mathbf{T}$ upon J must be considered explicitly. With the use of the $\mathbf{T}$ matrix, the angle-integrated cross section for a reaction going through $\alpha \to \alpha'$ is given as

$$\sigma_{\alpha\alpha'} = \frac{\pi}{k_\alpha^2}\sum_{Jll'ss'} g_J \left|T^J_{cc'}\right|^2, \tag{12}$$

where g_J is the statistical spin factor,

$$g_J = \frac{2J+1}{(2I_{\alpha 1}+1)(2I_{\alpha 2}+1)}, \tag{13}$$

and $I_{\alpha 1}$ and $I_{\alpha 2}$ are the projectile and target spins. It should be noted that the above equation does not hold for charged-particle elastic scattering.

2. *A-matrix approach*

The collision matrix given by Eqs. (8) and (9) is dependent upon the inversion of the channel matrix $(\mathbf{1} - \mathbf{RL_0})$. In the case of many levels and few channels, this task is computationally trivial. On the other hand, if a calculation includes many channels and few levels, the time necessary to perform the inversion is drastically increased. For this reason, it is useful to also define the collision matrix in terms of the *level* matrix, $A_{\lambda\lambda'}$. The relation is given by

$$U_{cc'} = \Omega_c\Omega_{c'}\left\{\delta_{cc'} + i\sum_{\lambda\lambda'}\Gamma^{\frac{1}{2}}_{\lambda c}\Gamma^{\frac{1}{2}}_{\lambda' c'}A_{\lambda\lambda'}\right\}, \tag{14}$$

where the matrix $A_{\lambda\lambda'}$ is defined by its inverse

$$(A^{-1})_{\lambda\lambda'} = (E_\lambda - E)\delta_{\lambda\lambda'} + \Delta_{\lambda\lambda'} - \frac{i\Gamma_{\lambda\lambda'}}{2}. \tag{15}$$

The additional quantities appearing in Eqs. (14) and (15) are

$$\Delta_{\lambda\lambda'} = -\sum_c \gamma_{\lambda c}\gamma_{\lambda' c}(S_c - B_c), \tag{16a}$$

$$\Gamma_{\lambda c} = 2P_c\gamma^2_{\lambda c}, \tag{16b}$$

and

$$\Gamma_{\lambda\lambda'} = \sum_c 2P_c\gamma_{\lambda c}\gamma_{\lambda' c}. \tag{16c}$$

While the use of the A matrix still requires an inversion, it is significantly less computationally intensive in the case of many channels and few levels. Once the collision matrix is obtained using Eq. (14), the calculation of the cross section follows through the procedure outlined above.

3. *Differential cross section*

The expression of the angle-integrated cross section in terms of the collision matrix is remarkably simple. For the differential cross section, a more rigorous calculation is involved. The differential cross section is related to the transition matrix by

$$\begin{aligned}(2s+1)\frac{k_\alpha^2}{\pi}\frac{d\sigma_{\alpha s,\alpha' s'}}{d\Omega_{\alpha'}} &= (2s+1)|C_{\alpha'}(\theta_{\alpha'})|^2\delta_{\alpha s,\alpha' s'} + \frac{1}{\pi}\sum_L B_L(\alpha s,\alpha' s') \\ &\quad\times P_L(\cos\theta_{\alpha'}) + \delta_{\alpha' s',\alpha s}(4\pi)^{-1/2}\sum_{Jl}(2J+1) \\ &\quad\times 2\mathrm{Re}\left[i\left(T^J_{c'c}\right)^* C_{\alpha'}(\theta_{\alpha'})P_l(\cos\theta_{\alpha'})\right].\end{aligned} \tag{17}$$

Several new quantities have been introduced in Eq. (17) to define the angular dependence of the cross section. The term $C_{\alpha'}(\theta_{\alpha'})$ represents the Coulomb amplitudes, while $P_L(\cos\theta_{\alpha'})$

are the Legendre polynomials. The remaining term is defined as

$$B_L(\alpha s, \alpha' s') = \frac{1}{4}(-1)^{s-s'} \sum_{J_1 J_2 l_1 l_2 l_1' l_2'} \bar{Z}(l_1 J_1 l_2 J_2, sL) \times \bar{Z}(l_1' J_1 l_2' J_2, s' L)\left(T^{J_1}_{\alpha' s' l_1', \alpha s l_1}\right)\left(T^{J_2}_{\alpha' s' l_2', \alpha s l_2}\right)^*, \quad (18)$$

with

$$\bar{Z}(l_1 J_1 l_2 J_2, sL) = (2l_1+1)^{1/2}(2l_2+1)^{1/2}(2J_1+1)^{1/2} \times (2J_2+1)^{1/2}(l_1 0 l_2 0|L0) W(l_1 J_1 l_2 J_2; sL). \quad (19)$$

The corresponding differential cross section formula in Ref. [21] (Eq. VIII.2.6) contains typographical errors; see Ref. [23] for further discussion. The specific differences are that a Kronecker delta has been applied to the third term, and the transition matrix has been conjugated. A final summation over the entrance and exit channel spins is necessary to calculate the differential cross section corresponding to the reaction $\alpha \to \alpha'$:

$$\frac{d\sigma_{\alpha,\alpha'}}{d\Omega_{\alpha'}} = \frac{1}{(2I_{\alpha 1}+1)(2I_{\alpha 2}+1)} \sum_{ss'} (2s+1) \frac{d\sigma_{\alpha s, \alpha' s'}}{d\Omega_{\alpha'}}. \quad (20)$$

4. Photon channels

The R-matrix theory described above is appropriate only for particle-particle reactions. In the internal region (enclosed by the boundary surface), photon channels can be included symmetrically with particle channels [21]; however, it has often been found necessary to include an additional capture component attributed to the external region (beyond the boundary radius).

In A-matrix formalism, the internal transition matrix element connecting a particle channel c to a photon channel $p \equiv \epsilon L \lambda_f$ takes the form

$$T^{J,\text{int}}_{cp} = -i \sum_{\lambda\lambda'} \Omega_c \Omega_p A_{\lambda\lambda'} \Gamma^{1/2}_{\lambda c} \Gamma^{1/2}_{\lambda' p}, \quad (21)$$

where

$$\Omega_p = 1, \quad \Gamma_{\lambda' p} = 2k_\gamma^{2L+1} \gamma^{\text{int}\,2}_{\lambda' p}. \quad (22)$$

In the above expression, the term λ_f indicates the final state with some defined energy and total spin J_f and L is the multipolarity of the γ-ray. The symbol ϵ has been introduced to indicate the mode of the emitted radiation, where $\epsilon = 0$ for magnetic transitions and $\epsilon = 1$ for electric transitions. It should be noted that the internal transition matrix can also be written in R-matrix formalism if photon channels are included in the definition of the R matrix, and the photon penetrability is defined to be $P_\gamma = k_\gamma^{2L+1}$. Additionally, it is also often assumed that the resonant state is not significantly dampened by the γ decay, therefore the elements of the diagonal matrix $\mathbf{L_0}$ are ignored for photon channels. In A-matrix formalism, this is tantamount to neglecting the photon channel from the channel sum in the definition of the A matrix. Such an assumption is not justified if the photon widths are appreciable compared to the particle widths, and in these cases proper photon channel damping must be included [21].

In the external region, the scattering state contains contributions from both resonant and hard-sphere phase shifts [24,25]. Throughout the remainder of this paper, the term EC will be associated with this nonresonant portion, while the external resonance contribution will be designated by ERC. Nonresonant capture has been treated historically in two distinct but analogous ways. The term direct capture (DC) often refers specifically to the formulation of Ref. [5], while the term EC, defined above, is associated with the hard-sphere formulation. With the assumption of the hard-sphere phase shift and a square-well bound-state potential in DC, the two formalisms become identical.

A full multilevel multichannel external capture theory was introduced in Ref. [14], and the formalism used in AZURE is based on that work. This approach allows resonant and direct or external capture contributions to be combined in a self-consistent manner. Additionally, we follow Ref. [15] and express the external capture in terms of the asymptotic normalization coefficient (ANC).

The following external capture equations apply for electric-multipole (EL) external capture transitions only, which are typically the most important cases in practice. The external portion of the transition matrix element is defined as

$$T^{J,\text{ext}}_{cp} = -i\Omega_c \sqrt{\frac{8(2L+1)(L+1)}{L\hbar}} \frac{k_\gamma^{L+1/2}}{(2L+1)!!} \times \left[\sum_{l_f} \frac{i^{l+L-l_f} \bar{e}^L_\alpha}{v_\alpha^{1/2}} (l0L0|l_f 0)\, U(Ll_f Js; lJ_f)\, R^{\text{EC}}_{cl_f L} + \sum_{c' l_f'} \frac{i^{l'+L-l_f'} \bar{e}^L_{\alpha'}}{v_{\alpha'}^{1/2}} (l'0L0|l_f' 0)\, U(Ll_f' Js'; l'J_f)\, R^{\text{ERC}}_{cc' l_f' L} \right], \quad (23)$$

where

$$\bar{e}^L_\alpha = e\left[Z_{\alpha 1} \left(\frac{M_{\alpha 2}}{A_\alpha}\right)^L + Z_{\alpha 2} \left(\frac{-M_{\alpha 1}}{A_\alpha}\right)^L \right] \quad (24)$$

is the effective charge term, with e the fundamental charge, $M_{\alpha i}$ and $Z_{\alpha i}$ are the constituent masses and charges of particle pair α, $A_\alpha = M_{\alpha 1} + M_{\alpha 2}$, and

$$U(Ll_f Js; lJ_f) = (2l+1)^{1/2}(2J_f+1)^{1/2} W(Ll_f Js; lJ_f)$$

is the *normalized* Racah coefficient. All quantities appearing with a subscript f refer to the final state configuration. It should be noted that our Eqs. (21) and (23) follow the sign convention of Refs. [21,25] and consequently differ from those of Ref. [14] by an overall minus sign (which has no effect upon observables). We have also allowed $\bar{e}^L_\alpha$ to depend upon the particle pair α, as it must if more than one pair type is present in the problem.

The integrals $R^{\rm EC}_{cl_fL}$ and $R^{\rm ERC}_{cc'l'_fL}$ contain the hard-sphere and resonant portions of the initial scattering wave function, respectively. The hard-sphere integral is given by

$$R^{\rm EC}_{cl_fL} = C_{\alpha s l_f}\int_{a_c}^{\infty} dr r^L \left[F_{\alpha l}(k_\alpha r)\cos\delta_c^{\rm hs} + G_{\alpha l}(k_\alpha r)\sin\delta_c^{\rm hs}\right] \times W_{-\eta_\alpha, l_f+1/2}(2k_{\alpha f} r). \quad (25)$$

In the above equation, the asymptotic normalization (ANC) is represented by $C_{\alpha s l_f}$, the functions $F_{\alpha l}(k_\alpha r)$ and $G_{\alpha l}(k_\alpha r)$ are normal Coulomb functions, $W_{-\eta_\alpha, l_f+1/2}(2k_{\alpha f} r)$ is a Whittaker function, and $\delta_c^{\rm hs}$ is the hard-sphere phase shift given by

$$\delta_c^{\rm hs} = -\tan^{-1}\left[\frac{F_{\alpha l}(k_\alpha a_c)}{G_{\alpha l}(k_\alpha a_c)}\right]. \quad (26)$$

The resonant external integral $R^{\rm ERC}_{cc'l'_fL}$ includes contributions from all channels. For open channels, we define

$$K_{Lcl_f} = \exp\left(i\delta_c^{\rm hs}\right) P_c^{1/2}\int_{a_c}^{\infty} dr\, r^L [G_{\alpha l}(k_\alpha r) + i F_{\alpha l}(k_\alpha r)] \times W_{-\eta_\alpha, l_f+1/2}(2k_{\alpha f} r), \quad (27)$$

and for closed channels

$$K_{Lcl_f} = (k_\alpha a_c)^{1/2}\int_{a_c}^{\infty} dr r^L \frac{W_{-\eta_\alpha, l+1/2}(2k_\alpha r)}{W_{-\eta_\alpha, l+1/2}(2k_\alpha a_c)} \times W_{-\eta_\alpha, l_f+1/2}(2k_{\alpha f} r). \quad (28)$$

In R-matrix formalism, the resonant external integral is given by

$$R^{\rm ERC}_{cc'l'_fL} = P_c^{1/2}[(\mathbf{1} - \mathbf{RL})^{-1}\mathbf{R}]_{cc'} C_{\alpha' s' l'_f} K_{Lc'l'_f}, \quad (29)$$

while for the A-matrix formalism the term takes the form

$$R^{\rm ERC}_{cc'l'_fL} = P_c^{1/2}\sum_{\lambda\mu}\gamma_{\lambda c}\gamma_{\mu c'} A_{\lambda\mu} C_{\alpha' s' l'_f} K_{Lc'l'_f}. \quad (30)$$

The above integrals can also be parametrized in terms of the dimensionless reduced width amplitude (DRWA), $\theta_{\alpha s l_f}$, by substituting for the ANC the expression

$$C_{\alpha s l_f} = \sqrt{\frac{2}{a_{\alpha s l_f}}}\theta_{\alpha s l_f}\frac{N_f^{1/2}}{W_{-\eta_\alpha, l_f+1/2}(2k_{\alpha f} a_c)}. \quad (31)$$

The normalization factor N_f results from the fact that R-matrix eigenfunctions are normalized to unity inside the channel radii. It is given by

$$N_f^{-1} = 1 + \sum_{\alpha s l_f}\frac{2\theta^2_{\alpha s l_f}}{a_{\alpha s l_f}}\int_{a_c}^{\infty}\left[\frac{W_{-\eta_\alpha, l_f+1/2}(2k_{\alpha f} r)}{W_{-\eta_\alpha, l_f+1/2}(2k_{\alpha f} a_{\alpha s l_f})}\right]^2 dr. \quad (32)$$

If the level shift of the final state vanishes, the dimensionless reduced width can be related to the R-matrix reduced width $\gamma_{\alpha s l_f}$ for that state via Eq. IV.3.10 of Ref. [21]:

$$\theta_{\alpha s l_f} = \frac{a_{\alpha s l_f}\sqrt{\mu_\alpha}}{\hbar}\gamma_{\alpha s l_f}, \quad (33)$$

and using Eq. A.29 of Ref. [21] the normalization factor can be written

$$N_f^{-1} = 1 + \sum_{\alpha s l_f}\gamma^2_{\alpha s l_f}\left(\frac{dS_{\alpha s l_f}}{dE}\right)_{a_{\alpha s l_f}}. \quad (34)$$

Alternative definitions of the dimensionless reduced width amplitude also exist.

Defining the total transition matrix element for capture as

$$T^J_{cp} = T^{J,\rm int}_{cp} + T^{J,\rm ext}_{cp}, \quad (35)$$

it can be shown that the differential cross section is given as

$$\frac{d\sigma_{\alpha\to\lambda_f}}{d\Omega} = \frac{1}{(2I_{\alpha 1}+1)(2I_{\alpha 2}+1)}\frac{1}{k_\alpha^2}\sum_k B_k P_k(\theta), \quad (36)$$

with the definitions

$$B_k = \sum_{s,L,L',l,l',J,J',\epsilon,\epsilon'}[\,]\frac{(-1)^{1+s-J_f}}{4} Z_1(lJl'J';sk) \times Z_2(LJL'J';J_f k) T^{*J'}_{\alpha s l',\epsilon' L'\lambda_f} T^J_{\alpha s l,\epsilon L\lambda_f}, \quad (37)$$

and

$$Z_1(lJl'J';sk) = \hat{l}\hat{l}'\hat{J}\hat{J}'(l0l'0|k0)W(lJl'J';sk), \quad (38a)$$

$$Z_2(LJL'J';J_f k) = \hat{L}\hat{L}'\hat{J}\hat{J}'(L1L'-1|k0)W(LJL'J';J_f k), \quad (38b)$$

where the symbol [ ] indicates a parity restriction defined by

$$[\,] = \tfrac{1}{2}[1 + (-1)^{L'+L+k+\epsilon+\epsilon'}]. \quad (39)$$

These equations are identical to those given in Ref. [26]. Integrating over the solid angle gives the usual expression for the total cross section:

$$\sigma_{\alpha\to\lambda_f} = \frac{\pi}{k_\alpha^2}\sum_{JlsL\epsilon} g_J\left|T^J_{cp}\right|^2. \quad (40)$$

B. Parameter transformations

Experimental resonance widths are usually presented as Breit-Wigner partial widths $\Gamma^o_{\lambda c}$, while R-matrix theory uses reduced width amplitudes $\gamma_{\lambda c}$ for the resonance parameters. The situation is complicated by the dependence of the reduced width amplitudes and R-matrix pole energies on the choice of boundary conditions. In R-matrix theory, a single set of fixed boundary conditions is defined for each J^π group of levels. The free parameters in the theory, namely, $\gamma_{\lambda c}$ and E_λ, are then fitted given this choice of boundary conditions. In the following section, the transformation from experimental to theoretical parameter space, and vice versa, is summarized.

In the discussion below, the notation of Ref. [18] has been adopted. Observed partial widths and level energies are denoted by $\Gamma^o_{\lambda c}$ and $\tilde{E}_\lambda$, respectively. The *on-resonance* reduced width amplitudes are represented by $\tilde{\gamma}_{\lambda c}$, while the R-matrix parameters transformed to a single boundary condition are given by $\gamma_{\lambda c}$ and E_λ. The definition of an *on-resonance* reduced width amplitude is inherently dependent upon a specific choice of boundary condition. Conventionally, the term *on-resonance* implies that the boundary condition for a given set of R-matrix parameters of a single level has been taken to be $S_c(\tilde{E}_\lambda)$, where

$\tilde{E}_\lambda$ is the observed level energy and S_c is the Coulomb shift function [21]. The descriptor *on-resonance* will be replaced by *physical* for the remainder of the discussion. Additionally, many of the formulas in the following sections include a sum over channels. The contribution from γ channels should be excluded from this summation [18].

1. Physical width amplitudes

For a single level, the observed width can be related to the physical reduced width amplitudes via [18]

$$\Gamma^o_{\lambda c} \equiv \frac{2P_c\tilde{\gamma}^2_{\lambda c}}{1+\sum_k \tilde{\gamma}^2_{\lambda k}\left(\frac{dS_k}{dE}\right)_{\tilde{E}_\lambda}}, \tag{41}$$

where P_c is the penetrability (Ref. [21], Eqs. XII.3.5 and XII.3.6). In the specialized case of photon channels, $P_c = k_\gamma^{2L+1}$ should be used in place of the Coulomb penetrability. In Eq. (41), a complete set of $\tilde{\gamma}_{\lambda c}$ parameters for a given level is assumed. As a result, this formula can be inverted to yield a single physical reduced width amplitude using

$$\tilde{\gamma}^2_{\lambda c} = \frac{\Gamma^o_{\lambda c}}{P_c}\left[2-\sum_k \frac{\Gamma^o_{\lambda k}}{P_k}\left(\frac{dS_k}{dE}\right)_{\tilde{E}_\lambda}\right]^{-1}. \tag{42}$$

While these formulas dictate the transformation from observed partial widths to physical reduced width amplitudes, additional conventions are needed to shift the boundary condition dependence of the parameter space in R-matrix theory.

2. Brune transformation

A process has been suggested in Ref. [18] to further transform the $\tilde{\gamma}_{\lambda c}$ and $\tilde{E}_\lambda$ parameters of multiple levels relative to a single boundary condition in R-matrix space. This is extremely useful to determine initial parameters for an R-matrix fit from literature values. It is first necessary to define two square level matrices, **M** and **N**, as

$$M_{\mu\lambda} = \begin{cases} 1 & \text{for} \quad \mu = \lambda, \\ -\sum_c \tilde{\gamma}_{\mu c}\tilde{\gamma}_{\lambda c}\frac{S_{\mu c}-S_{\lambda c}}{\tilde{E}_\mu - \tilde{E}_\lambda} & \text{for} \quad \mu \neq \lambda, \end{cases} \tag{43}$$

and

$$N_{\mu\lambda} = \begin{cases} \tilde{E}_\mu + \sum_c \tilde{\gamma}^2_{\mu c}(S_{\mu c}-B_c) & \text{for} \quad \mu = \lambda, \\ \sum_c \tilde{\gamma}_{\mu c}\tilde{\gamma}_{\lambda c}\left(\frac{\tilde{E}_\mu S_{\lambda c}-\tilde{E}_\lambda S_{\mu c}}{\tilde{E}_\mu - \tilde{E}_\lambda} - B_c\right) & \text{for} \quad \mu \neq \lambda. \end{cases} \tag{44}$$

In these equations, $S_{\mu c}$ denotes the shift function for a given channel evaluated at the pole energy $\tilde{E}_\mu$, where the boundary condition for which this transformation is relevant is B_c. The transformed reduced width amplitudes result from a solution to the eigenvalue equation

$$\mathbf{N}\boldsymbol{b_v} = E_v\mathbf{M}\boldsymbol{b_v}, \tag{45}$$

where E_v is the transformed R-matrix pole energy. The transformation for the reduced width amplitudes then follows from

$$\gamma_{vc} = \boldsymbol{b}_v^T\tilde{\boldsymbol{\gamma}}_c, \tag{46}$$

where $\tilde{\boldsymbol{\gamma}}_c$ is a channel vector with components corresponding to each level in the J^π grouping.

3. Barker transformation

At the conclusion of the fitting process, it is useful to reinstate the $B_c = S_c(\tilde{E}_\lambda)$ boundary condition dependence for each individual set of level parameters prior to converting reduced width amplitudes to observed partial widths. In Ref. [17], a proposed method inverts the procedure described in Sec. II B2. A level matrix **C** is defined as

$$C_{\mu\lambda} = E_\mu\delta_{\mu\lambda} - \sum_c (B'_c - B_c)\gamma_{\mu c}\gamma_{\lambda c}, \tag{47}$$

where B_c is the single boundary condition corresponding to the set of R-matrix parameters resulting from the fit, and B'_c is the boundary condition for the transformed parameters. It is then required to find an orthogonal matrix **K** such that **C** is diagonalized by the transformation

$$\mathbf{D} = \mathbf{KCK^T}. \tag{48}$$

The diagonal elements of **D** contain the eigenvalues (which are the transformed E'_v) of **C**, while the column vectors of $\mathbf{K^T}$ make up the corresponding eigenvectors ($\boldsymbol{k}_v^T$). The transformation of the reduced width amplitude to the new boundary condition then follows from

$$\gamma'_{vc} = \boldsymbol{k}_v\boldsymbol{\gamma}_c \quad \text{or} \quad \boldsymbol{\gamma}'_c = \boldsymbol{K}\boldsymbol{\gamma}_c. \tag{49}$$

A set of parameters for a single level are denoted as physical when $B_c = S_c(\tilde{E}_\lambda)$, though $\tilde{E}_\lambda$ is initially unknown. If $B'_c = S(E_\lambda)$ is adopted as an initial estimate, and the process is repeated iteratively, the transformation most often converges to a set of parameters relative to the desired boundary condition. This process must subsequently be repeated for each level in a given J^π grouping. With a complete set of physical R-matrix parameters, a conversion to a complete set of observed partial widths can be determined using Eq. (41).

III. AZURE

AZURE is a multichannel, multilevel R-matrix computer code written in FORTRAN 77. It is designed to model low-energy nuclear reactions involving charged particles, γ rays, and neutrons. The main focus is to extract level energies, observed partial widths, and bound state normalization parameters (ANCs or DRWAs) from the analysis of experimental excitation functions and angular distributions, and to determine S factors at or near the energies of interest to nuclear astrophysics.

The AZURE package is divided into two primary subroutines, linked by the fitting package MINUIT [27]. In the first subroutine, all quantities that are not dependent on the R-matrix parameter sets are calculated. The second subroutine, called iteratively by the MINUIT package, calculates the cross section from the R-matrix parameters and applies beam and target effects to determine the total χ^2 value.

A graphical user interface (GUI) has been developed to expedite data management and program configuration. The

user can add or delete entire reaction channels, turn on, turn off, or edit resonances and their associated parameters, as well as swap data sets in and out. In addition, many analysis options within AZURE are controlled by configuration flags, which can be toggled using the GUI.

The multichannel aspect permits the inclusion of as many channels as allowed by angular momentum conservation for as many compound state decay reactions as desired. At the present time, AZURE permits simultaneous analysis of reactions occurring through only a single entrance particle pair. All allowed interferences are automatically taken into account. This allows for more strict constraints on the fitted parameters, but introduces additional demands on the relative energy calibrations and target thickness corrections for the data sets for different reactions and experiments. Also, both nonresonant EC and resonant ERC external channel capture have been implemented in AZURE using this full multichannel approach.

The matrix transformations of Brune and Barker (See Sec. II B) are implemented in AZURE. Therefore, it is possible to use experimental resonance energies and widths directly as starting parameters. These are automatically converted into the proper reduced width amplitudes and pole energies and, following the R-matrix analysis, are transformed back into physical parameters. AZURE utilizes the package LAPACK [28] to solve the eigensystems necessary for the transformations.

Many other analysis options are also available in AZURE, including, but not limited to, target integration, beam energy convolution, and inverse kinematics. The technical and computational aspects of AZURE are described in the AZURE user manual which is accessible on the AZURE website. The source code for AZURE, the graphical user interface, and the user manual are available online at http://azure.nd.edu/. Several examples are also included to demonstrate the various features offered by the AZURE code.

IV. EXAMPLES AND APPLICATIONS

In this section, the application of AZURE for the analysis of a number of proton-induced scattering and radiative capture reactions will be presented. The focus will be on three key reactions in the first and second CNO cycles [19,20]. The reactions are selected, in part, to demonstrate the versatility of the code. For the examples in this study, the data were taken from published reports only. This allows a better comparison to be made with the results of previous reaction analysis.

In R-matrix analysis of low-energy cross sections, the fitted results often depend on the value chosen for the radius parameter a_c. In the first example, an error analysis has been performed to explore the radial dependence of the R-matrix parameters for this reaction. In the other cases, the value of a_c is chosen to be that of the previous relevant publications to allow a direct comparison of the resulting reaction parameters.

The $^{12}C(p,\gamma)^{13}N$ radiative capture cross section is characterized by broad resonances and a nonresonant direct capture component which leads to pronounced interference effects over the entire observed energy range. In this example, the elastic scattering channel was evaluated simultaneously to enhance the constraints on the particle widths. The $^{14}N(p,\gamma)^{15}O$ reaction, on the other hand, is characterized by very narrow resonances and a continuous direct capture component which locally causes interference effects in the cross sections. The final example reaction $^{16}O(p,\gamma)^{17}F$ is completely dominated by a nonresonant direct capture reaction mechanism without significant resonant contributions.

With the exception of bound state energies, all parameters given in the tables of the following examples have been left free in the fit unless otherwise indicated.

A. $^{12}C + p$ reaction

The $^{12}C(p,\gamma)^{13}N$ reaction is critical to understanding stellar hydrogen burning in massive stars. It initiates the first CNO cycle, or the CN cycle, on the available ^{12}C seed abundance in the stellar material [19]. There have been extensive measurements in the past mapping the cross section in the energy range from 2.3 MeV down to 0.15 MeV [6,29]. These results indicate that at astrophysical energies, the cross section of $^{12}C(p,\gamma)^{13}N$ is dominated by the low-energy tail of a $J^\pi = 1/2^+$ resonance at $E_p = 461$ keV and an $E1$ external capture component arising from $s \rightarrow p$ and $d \rightarrow p$ orbital transitions. Previous analysis predicts a low-energy total S factor of $S \approx 1.5$ keV barn at 25 keV [30], which is comparable to the low-energy S factor of $^{14}N(p,\gamma)^{15}O$, the slowest reaction of the CN cycle.

Because of the complex interplay of a strong direct nonresonant component with a large resonant component at astrophysical energies, the $^{12}C(p,\gamma)^{13}N$ reaction is an excellent demonstration of the versatility of the AZURE code. As the low-energy capture data adopted in the following fits originated directly from Ref. [29], and therefore contain no uncertainties from digitization, this example is also used to highlight the sensitivity studies which can be performed with AZURE to evaluate the uncertainties in both fit parameters and extrapolations.

1. Experimental data and R-matrix analysis

In the present analysis, capture data for the $^{12}C(p,\gamma)^{13}N$ reaction from Refs. [6,29] were initially considered. Additionally, available elastic scattering data from Ref. [31] were included to further constrain the entrance channel. While the capture data of Ref. [6] represent the most extensive low-energy measurement to date, questions have arisen in the literature [30,32,33] concerning the reliability of the data extracted from the figures in the publication. Notably, a discrepancy in the energy of the $J^\pi = 3/2^-$ resonance has been reported in Refs. [32,33], where it was observed that the resonance at $E_p = 1689$ keV disagrees with the quoted energy of $E_p = 1699$ keV of Ref. [6]. An energy of $E_p = 1689 \pm 2$ keV was later adopted in Ref. [34]. An AZURE fit to a digitized data set of Ref. [6] yielded $E_p = 1709$ keV. A separate AZURE fit to the elastic scattering data of Ref. [31] positions the resonance at $E_p = 1686$ keV, in better agreement with previous results [32–34]. In light of this discrepancy, and considering the negligible effect of this resonance at astrophysical energies, only the data of Ref. [29] extending

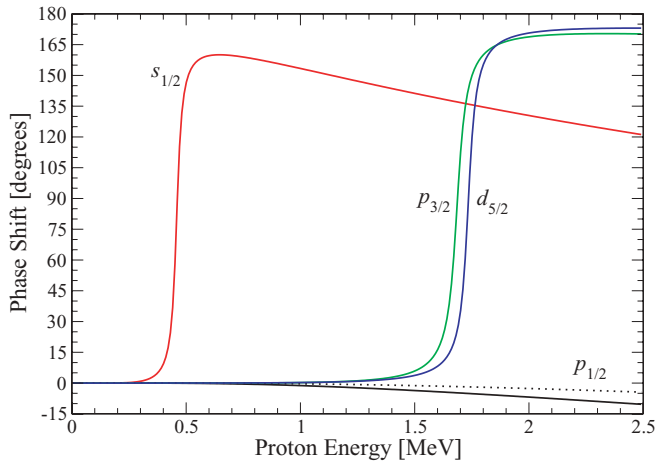

FIG. 1. (Color online) Calculated nuclear phase shifts for the $^{12}C + p$ reaction. The solid black line indicates the total $p_{1/2}$ phase shift including the ground state contribution, while the dotted black line represents only the hard-sphere phase shift.

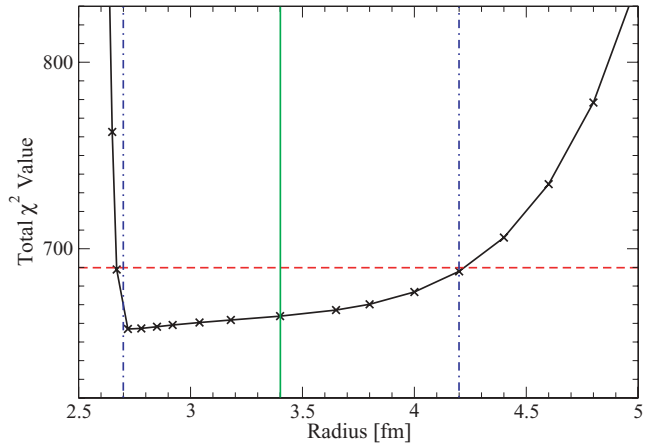

FIG. 2. (Color online) Scan of the best fit χ^2 value as a function of the entrance channel radius. The vertical green (solid) line indicates the adopted value, while the vertical blue (dash-dotted) lines correspond to a 5% variation from the minimum χ^2 value (horizontal red dashed line).

up to $E_p = 685$ keV have been used in the present analysis. The data resulting from the study in Ref. [29] are directly listed in the thesis; the use of these data helped avoid errors resulting from scanning and digitization of data figure representations. While the resonant contribution of the $J^\pi = 3/2^-$ state is unimportant at astrophysical energies, capture in this energy range exhibits strong interference with the external direct component. New data for the $^{12}C(p,\gamma)^{13}N$ reaction in this energy region could serve to further constrain the direct contribution.

The data of Ref. [29] were fitted simultaneously with the elastic scattering data of Ref. [31]. A renormalization was applied to the capture data to reproduce a peak cross section for the $J^\pi = 1/2^+$ resonance of 102 ± 8 μb recommended in Ref. [30]. In addition to this resonance, the state at $E_p = 1686$ keV ($J^\pi = 3/2^-$) and an additional state $E_p = 1735$ keV ($J^\pi = 5/2^+$) were included in the scattering channel. While these states were not included in the capture channel for the final analysis, tests were performed to ensure nonzero capture widths would have a negligible contribution to the fit. The above-mentioned external capture contributions were also incorporated. Though not observable directly in the capture channel, a subthreshold contribution from the ground state is needed to properly fit the elastic scattering data [31]. Figure 1 shows the nuclear phase shifts calculated from the best fit parameters. The effect of the $p_{1/2}$ ground state inclusion only becomes significant in the region of the two higher energy $p_{3/2}$ and $d_{5/2}$ resonances, therefore no interference contribution is expected in the differential cross section around the lower $s_{1/2}$ resonance. The proton reduced width amplitude of this subthreshold state is directly convertible to the ANC used to normalize the external capture contribution, therefore these two contributions were fitted with a single parameter. A channel radius of $a_c = 3.4$ fm was adopted. Figure 2 shows the variation of the total minimum χ^2 value with respect to the channel radius. All radii producing a best fit χ^2 value within 5% of the minimum were considered acceptable, corresponding to an allowed range for the channel radius of 2.7–4.2 fm. Fits to the capture and scattering data are shown in Fig. 3 and Figs. 4 and 5, respectively. In Fig. 3, the best fit not including external capture is shown, highlighting the importance of this reaction mechanism. The constraint of the ground state ANC by the scattering channel can be seen in Fig. 5, where a fit not including the subthreshold contribution is also given. The effect is most pronounced at $\theta_{c.m.} = 118.9°$.

2. *Astrophysical S factor at 25 keV*

A scan of the $S(25\,\text{keV})$ value as a function of channel radius was performed, and a maximum variation of approximately 1% was found. The uncertainty of the AZURE extrapolation was evaluated by placing a fictitious data point with negligible uncertainty at the energy of interest, varying the magnitude of this data point, and observing the net effect on the χ^2 value of the best fit as a function of the extrapolated

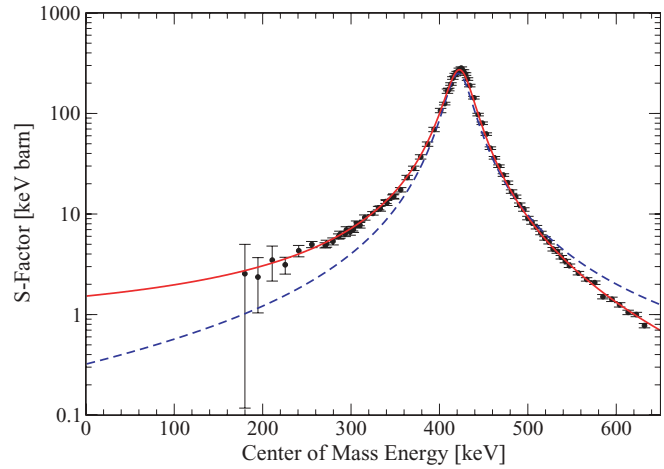

FIG. 3. (Color online) AZURE fit to the $^{12}C(p,\gamma)^{13}N$ data of Ref. [29]. The red (solid) line indicates the best fit including external capture, while the blue (dashed) line is the best fit if external capture is neglected.

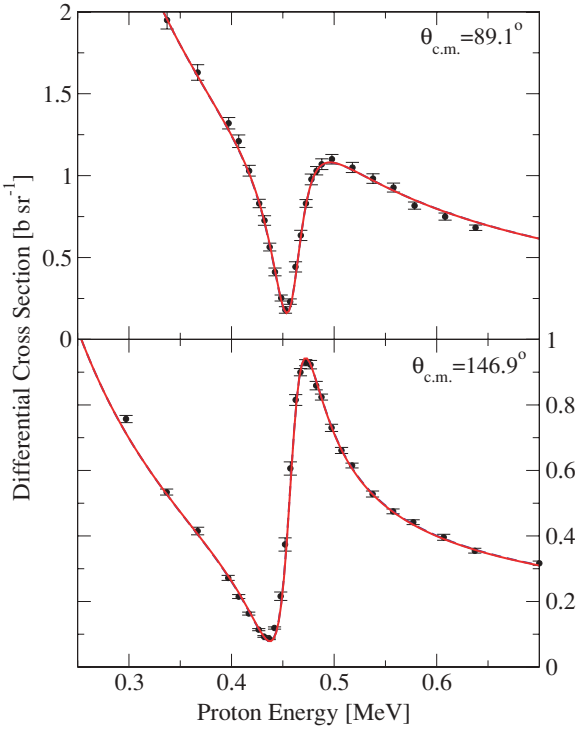

FIG. 4. (Color online) AZURE fit to the low-energy ^{12}C(p, p)^{12}C data of Ref. [31].

S factor. The effect of the fictitious point on the overall χ^2 determination was extracted. An allowed variation of 5% from the minimum χ^2 value contributes a 10% uncertainty in the

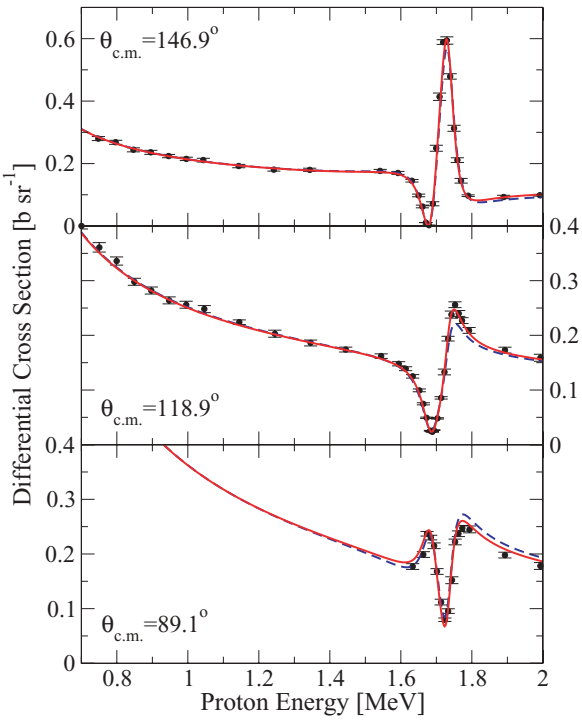

FIG. 5. (Color online) AZURE fit to the high-energy ^{12}C(p, p)^{12}C data of [31]. The red (solid) line indicates the best fit with the inclusion of the ground state as a subthreshold component, while the blue (dashed) line is the best fit excluding this contribution.

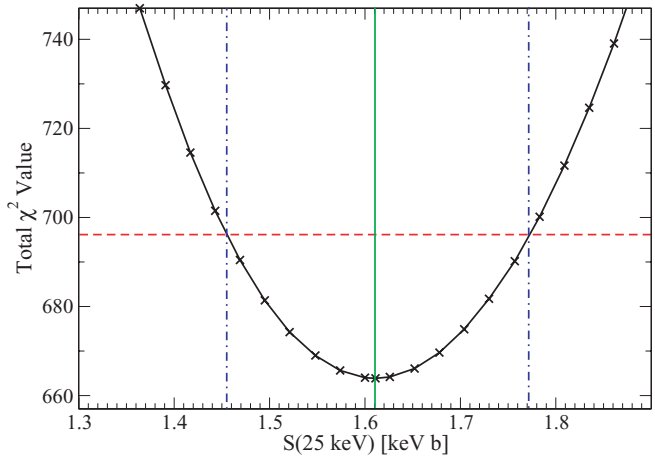

FIG. 6. (Color online) Scan of the best fit χ^2 value as a function of S(25 keV). The green (solid) line indicates the adopted value, while the blue (dash-dot) lines correspond to a 5% variation from the minimum χ^2 value (red dashed line). The half-width of the parabola at the 5% line corresponds to approximately 10%.

S(25 keV) extrapolation (see Fig. 6). Coupling this with the error in channel radius gives an overall fit uncertainty in the extrapolated S(25 keV) value of 11%. In Ref. [30], the authors quote an uncertainty in their overall capture normalization of ± 8 μb, yielding a systematic uncertainty for S(25 keV) of an additional 8%. Taking all of these uncertainties into account produces a final extrapolated value of $S(25\ \text{keV}) = 1.61 \pm 0.29$ keV b. This extrapolated S(25 keV) value is in good agreement with the value of $S(25\ \text{keV}) = 1.54$ keV b recommended in Ref. [30]. Comparison with other S factor predictions on the basis of previous work such as in Ref. [6] would require a renormalization of their results according to the suggestions made in Ref. [30] and has not been performed here.

3. *Reaction parameter description and comparison*

Table I shows the parameters of the present best fit. The physical proton widths, indicated as Γ_p^0, were evaluated with the boundary condition equal to the shift function at the energy of the resonance. It should be noted that the physical and formal R-matrix parameters are identical in this case given that there is only a single level per J^π group. The notation γ_γ(int) indicates the internal reduced width amplitude of the γ channel. External resonance capture also contributes to this level, but is completely determined by the proton reduced width amplitude of the level and the ANC of the ground state. The base uncertainties given in the table correspond to a 5% increase in the minimum χ^2 value of the best fit with respect to the variation of a single parameter, a process which can be automated using MINUIT. While the R-matrix parameters are particularly dependent on the choice of boundary radius, a radial change of less than 1% was found after the conversion to physical widths and has been included in the estimation of the uncertainty for these values. The fitted ANC for the ground state also displayed less than a 1% variation over the allowed radii. The uncertainty quoted in Ref. [30] in the overall normalization of the capture data contributes an additional variation of

TABLE I. Physical best fit parameters for the $^{12}C + p$ reaction. A channel radius of $a_c = 3.4$ fm was used in the fit.

E_λ (keV)	E_p (keV)	γ_p (MeV$^{-1/2}$)	Γ_p^0 (keV)	γ_γ (int) (MeV$^{-1/2}$)
0.000	−2107	1.84 ± 0.24	$C_{p1/2} = 1.87 \pm 0.24$ fm$^{-1/2}$	–
2370 ± 3	461 ± 3	2.83 ± 0.12	34.1 ± 0.8	0.500 ± 0.125
3500 ± 1	1686 ± 1	0.570 ± 0.008	57.9 ± 1.7	–
3545 ± 2	1735 ± 2	2.38 ± 0.08	48.3 ± 1.9	–

approximately 4% in the fitted ground state ANC and internal γ width of the 461 keV resonance. The internal γ width for this state is not well constrained in the present fit because of the indistinguishable mixing of internal and external contributions. New measurements over a larger energy range would serve to better establish the external contribution and would in turn lower the uncertainty of the internal width. The present physical proton widths for the unbound states agree within 6% of the values quoted in Ref. [31], while the physical energies of the resonances are confirmed within 0.5%. The ANC derived in the present fit is also in good agreement with the indirect value of $C_{p1/2} = 1.81 \pm 0.07$ fm$^{-1/2}$ measured in Ref. [35].

The excellent agreement of the AZURE fit with previous R-matrix and external capture analysis of the $^{12}C + p$ reaction serves as a strong confirmation of the reliability of the code. The multichannel nature of the present analysis demonstrates the power of AZURE to constrain the parameter space of a fit through the incorporation of multiple reactions accessing the same compound nucleus.

B. $^{14}N(p,\gamma)^{15}O$ reaction

The radiative capture process $^{14}N(p,\gamma)^{15}O$ is considered the most critical reaction in the CNO cycles. At temperatures typical for core hydrogen burning in stars, the reaction is the slowest in the entire cycle and therefore determines the overall fusion rate of four protons to one α particle. Consequently, it is this reaction which determines the energy production for hydrogen burning in massive stars. Furthermore, this rate determines the time scale for main sequence stars (with masses $M \geqslant 2M_\odot$) and has been used to determine the age of globular clusters [36]. More recently it has been argued that good knowledge of the reaction rate is necessary to determine the core metallicity of the Sun from direct observation of CNO neutrinos associated with the decay of ^{13}N, ^{15}O, and ^{17}F [37].

The total reaction cross section is determined by a number of reaction components including external direct capture, subthreshold states, low-energy tails from a number of resonances, and different interference terms between resonant and nonresonant reaction contributions. The reaction proceeds most strongly by external capture to the 6.79 MeV ($J^\pi = 3/2^+$) excited state and by resonant and external capture to the ground state ($J^\pi = 1/2^-$) and 6.18 MeV ($J^\pi = 3/2^-$) excited state, with several additional transitions to excited states at 5.18, 5.24, 6.86, and 7.28 MeV contributing weakly at low energies. There have been a number of attempts in the past [15,38–41] to analyze the reaction cross section data in the framework of a single channel R-matrix model. In R-matrix theory, any decay of the compound nucleus leading to a different final state is represented by an additional set of channels. The many distinct transitions in this reaction, as well as the complex interplay between various external and resonant components, make it an excellent demonstration of the multichannel, multilevel capabilities of AZURE.

1. *Experimental reaction data*

The broadest set of measurements, in terms of the number of transitions identified and the energy range covered (0.2–2.5 MeV), were made by Schröder *et al.* [42]. Angulo and Descouvemont [15] reanalyzed this data set and obtained a significantly smaller $S(0)$ than Schröder *et al.*, primarily because of a weaker contribution for the subthreshold level in the ground state transition. The data of Ref. [42] were subsequently corrected for summing effects in Ref. [43]. In two recent experiments from the LUNA [38,40] and LENA [39] collaborations, the yield curves were remeasured, focusing on the low-energy region. These works reached different conclusions on the low-energy S factors for the different primary transitions, particularly the ground state transition, but the total S factors were in reasonable agreement. These differences in the R-matrix fits prompted a remeasurement of the ground state transition near 0.3 MeV [41], this energy being expected to offer the best constraint on the S factor at astrophysical energies. The lowest energy measurements of the $^{14}N(p,\gamma)^{15}O$ reaction were reported in Refs. [44,45], where the transition-inclusive $(p,\gamma_{\text{total}})$ cross section was measured; and while not included in the χ^2 fit in the present analysis, we compare the sum of our primary transition fits to these data.

In addition to the direct measurement of cross sections, the lifetime of the important 6.792 MeV state was measured using the Doppler-shift attenuation method [46,47] and via Coulomb excitation [48]. The strong external capture components in several transitions led to measurements of the asymptotic normalization coefficients using the $^{14}N(^3He,d)^{15}O$ transfer reaction [35,49,50]. The analyzing power and inferred $M1$ contributions were measured in the 6.18 and 6.79 MeV transitions [51], though in Ref. [39] the effect of the suggested $M1$ background component in the 6.18 MeV transition was found to be negligible.

2. *Selection of resonances, transitions, and parameters for the R-matrix analysis*

The yield curves show the presence of $J^\pi = 1/2^+$ resonances at center-of-mass energies 0.259 and 1.45 MeV and $J^\pi = 3/2^+$ resonances at −0.504 (subthreshold), 0.985, and 2.19 MeV. A $J^\pi = 3/2^+$ background pole was included for the ground state transition. Resonance energies and widths were

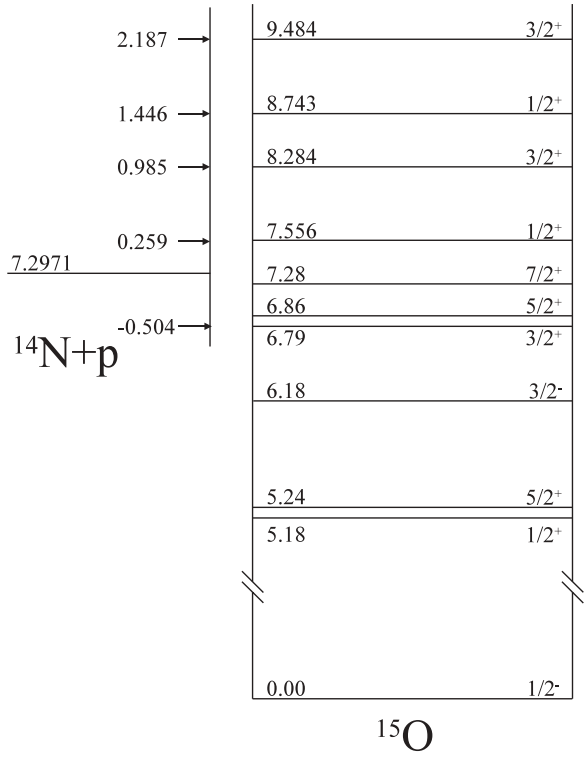

FIG. 7. ^{15}O compound nucleus level scheme indicating the relevant resonances and final states for the resonant and external capture induced γ transitions in radiative proton capture on ^{14}N.

fixed to literature values, with the exceptions stated below. ANCs were left as free parameters except in the ground state transition, where the external capture contribution is believed to be weak and is obscured by other nonresonant components. The resonances and final states are summarized in Fig. 7. For all fits, a radius parameter of $a = 5.5$ fm was adopted from previous R-matrix studies [15,39–41] to allow for a direct comparison of the AZURE reaction parameters with literature results.

For resonance capture, it was assumed that only the lowest incident ℓ_i value and multipolarity L would contribute. This assumption is investigated in the ground state transition, where there is strong destructive interference in the $\ell_i = 0$ contributions at low energies. For external capture, $1/2$ and $3/2$ channel spin contributions are allowed, and the lowest two incident ℓ_i values as appropriate. The initial values for the ANCs are taken from Ref. [50], converted to the present coupling scheme, and are denoted by $C_{\ell_f I}$, where ℓ_f is the final state orbital angular momentum and I the channel spin.

At low energies, the ground state transition is primarily determined by the interference between different $J^\pi = 3/2^+$ reaction components, which include the subthreshold state, the broad 2.19 MeV resonance, the background pole, and the external capture contribution. The proton reduced width amplitude γ_p of the subthreshold state was fixed using the ANC $C^{6.79}_{s3/2} = 4.7$ fm$^{-1/2}$ [40]. In addition, the ANC for the ground state external capture was fixed at $C^{0.00}_{p3/2} = 7.3$ fm$^{-1/2}$. These values are taken from previous R-matrix analyses [40] and indirect determinations [50]. The weaker $I = 1/2$ external capture component was fixed using the ANC of Ref. [50]. The widths of the narrow resonance at 0.259 MeV were left as free parameters, while the proton width Γ_p of the 0.985 MeV resonance was fixed at 3.0 keV. The energy of the $J^\pi = 3/2^+$ background pole was set at $E_{c.m.} = 6$ MeV, with a proton width of $\Gamma_p = 8$ MeV. The γ partial widths Γ_γ of the subthreshold state and background pole, along with the width of the 2.19 MeV resonance were treated as free parameters, which determined the broad resonance contributions.

Capture to the 6.79 MeV state shows a strong $I = 3/2$ external capture component added incoherently to the 0.259 MeV resonance. The ANC of the 6.79 MeV $J^\pi = 3/2^+$ state, and the related proton reduced width amplitude γ_p, relevant for the ground state transition, were treated as independent parameters in the fitting procedure.

For the 5.18 and 6.18 MeV transitions, the $J^\pi = 1/2^+$ resonances at 0.259 and 1.45 MeV and the $J^\pi = 3/2^+$ resonance at 0.985 MeV were included. The transition to the 6.18 MeV state also includes $I = 1/2$ and $I = 3/2$ external capture contributions. The proton width Γ_p and the capture widths Γ_γ of the 1.45 MeV resonance were fixed, as the widths of this resonance are not well defined by the existing data at higher energies [42].

The 5.24, 6.86, and 7.28 MeV states all contribute weakly at astrophysical energies, are strongly nonresonant, and were modeled as external capture transitions. The transitions to the 5.24 and 6.86 MeV states also included the 0.985 and 2.19 MeV resonances.

3. *Single-channel R-matrix analyses of the ground state transition*

The primary transition with the largest uncertainty is to the ground state, and a variety of $S_{0.00}(0)$ values have been obtained often based on different data sets and different R-matrix techniques. Generally it has been assumed that only the lowest entrance channel angular momentum ℓ_i will contribute, though it was noted in Ref. [15] that $\ell_i = 2$ contributions may be significant for the 2.19 MeV resonance, as indicated by elastic scattering experiments, e.g., Refs. [52,53]. While the significance of d-wave components at low energy may be very small, the dominant broad s-wave components are sensitive to the data at energies where the d-wave components could be non-negligible.

Previous R-matrix fits [38–41] were reproduced in the present work by fitting the appropriate data subsets using similar fitting procedures, in order to verify the AZURE code. The following is a brief summary of the previous analyses.

In the fits of Ref. [38], the new low-energy data and the higher energy data of Ref. [42], corrected for summing effects were used. For the fit of Ref. [39], only the data from that study were used; and though contributions from the 2.19 MeV background resonances were included, the widths and energies were fixed to the values of Ref. [15]. In the fits of Ref. [41], the only data set used in addition to their own was that of Schröder *et al.*, neglecting the data of Refs. [38,39] because of the possible uncertainties in the large summing corrections.

Such a selective choice of data sets by these references may explain the differences in the S-factor predictions for the ground state transition. The present study seeks to address this

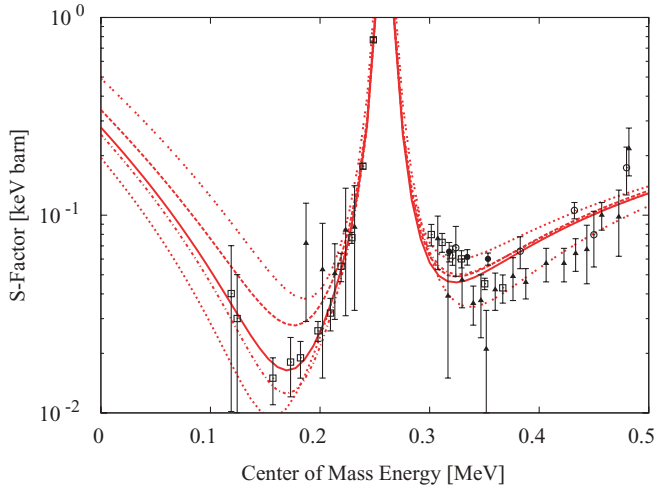

FIG. 8. (Color online) Fits to the ground state transition in the low-energy region to match those from Refs. [38,40] (dot-dash), [39] (dot-dot), and [41] (dotted). AZURE fits to all the data using the lowest ℓ_i assumption are shown (solid), along with fits allowing $\ell_i = 2$ for the external capture and 2.19 MeV resonance (dashed). The data shown are from Refs. [42] (open circles), [38] (open squares), [39] (solid triangles), and [41] (solid circles).

by providing a comprehensive fit analysis to all available data. The analysis is constrained by including only the minimum ℓ_i contributions. For exploring the possibility of higher ℓ_i components as suggested in Ref. [15], this assumption was relaxed for the 2.19 MeV resonance and the external capture contribution.

Figure 8 shows the resulting fits as described above. The fits from previous studies are well reproduced, with the current fit ($\ell_i = 0$) to all available data being closest to that from Ref. [38]. The primary source of the difference is likely the inclusion of the data of Ref. [39] in the present fits, which lowers the fit in the 0.3–0.4 MeV region. The inclusion of $\ell_i = 2$ contributions has little effect on the high-energy side of the 0.259 MeV resonance but results in a considerably larger S factor below 0.2 MeV in disagreement with the lowest energy LUNA data, thereby demonstrating that such a component could have an effect on the astrophysical reaction rate and requires further study.

4. *R-matrix multichannel analysis for all transitions*

This section demonstrates the multichannel fit capability of AZURE; it presents the results of a simultaneous R-matrix analysis for all seven observed transitions in the $^{14}\mathrm{N}(p,\gamma)^{15}\mathrm{O}$ radiative capture reaction.

The ground state transition was fitted including only the lowest ℓ_i. The resulting multichannel fit for the ground state transition is shown in Fig. 9, and is essentially identical to the single-channel fits described in the previous section. The resulting $S_{0.00}(0) = 0.28$ keV b is slightly larger than the result of [38] $S_{0.00}(0) = 0.25 \pm 0.06$ keV b. This change is most likely due to the inclusion of the data from Ref. [39] in the present study, since the low-energy extrapolation is very sensitive to the data on the upper side of the 0.259 MeV resonance.

The fitted value for $\Gamma_\gamma^{0.00}$ (int) for the subthreshold state is 0.62 eV, in good agreement with the values of Refs. [46]

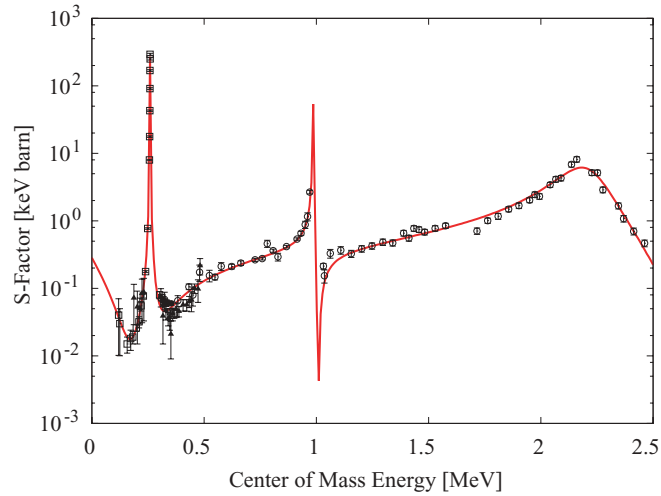

FIG. 9. (Color online) AZURE fit for the ground state transition. The solid line shows the current fits to the data of Refs. [42] (open circles), [38,40] (open squares), [39] (solid triangles), and [41] (solid circles).

$0.41^{+0.34}_{-0.13}$ eV, [48] $0.95^{+0.60}_{-0.95}$ eV, and [47] > 0.85 eV, though how well the internal width is constrained by the current analysis is unclear.

Current fits for the transition to the 6.18 MeV state, shown in Fig. 10, describe the data well, particularly around the 0.259 MeV resonance. The fitted ANC of $C_{p1/2} = 0.49$ fm$^{-1/2}$ compares excellently to that of Refs. [50] 0.47 ± 0.03 fm$^{-1/2}$ and [49] 0.45 ± 0.05 fm$^{-1/2}$, but is larger than the value determined from a previous R-matrix analysis of $C_{p1/2} = 0.2 \pm 0.1$ fm$^{-1/2}$ [40]. This may be due to our inclusion of the channel spin $I = 3/2$ component, the fitted ANC of which $C_{p3/2} = 0.36$ fm$^{-1/2}$ compares reasonably to the results of Refs. [50] 0.53 ± 0.03 fm$^{-1/2}$ and [49] 0.51 ± 0.06 fm$^{-1/2}$. The extrapolated $S_{6.18}(0) = 0.12$ keV b is somewhat larger than 0.08 ± 0.03 keV b from Ref. [40], but is in excellent agreement with that from Refs. [50] $S_{6.18}(0) = 0.13 \pm 0.02$

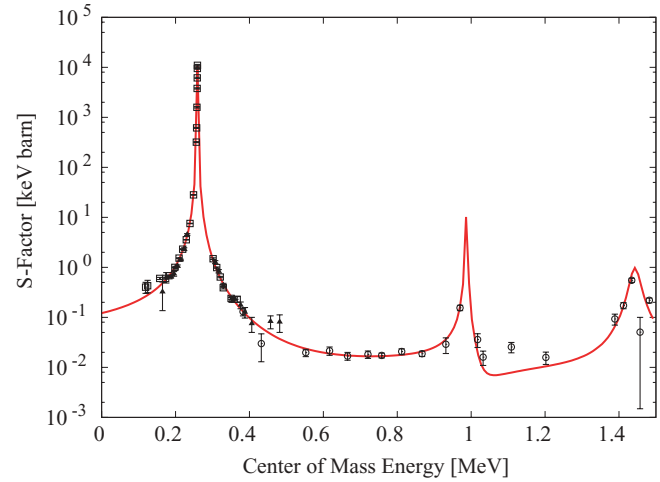

FIG. 10. (Color online) Fits for the 6.18 MeV state transition. The data sets are from Refs. [42] (open circles), [40] (open squares), and [39] (solid triangles).

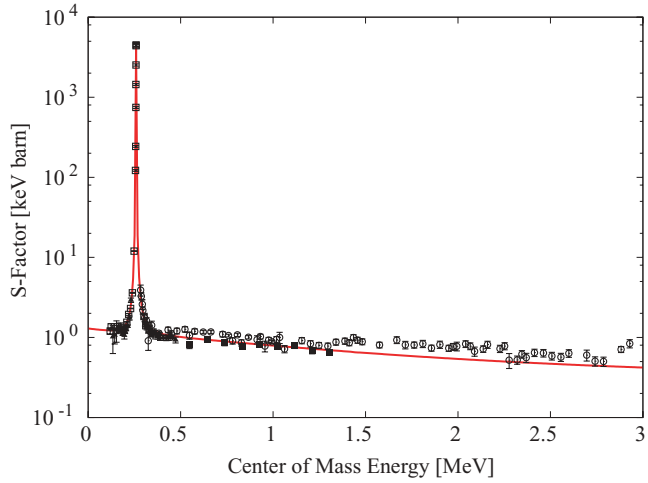

FIG. 11. (Color online) Fit for the 6.79 MeV final state transition. The data are from Refs. [42] (open circles), [38] (open squares), and [39] (solid triangles), and data taken in Bochum (solid squares, see Ref. [40]).

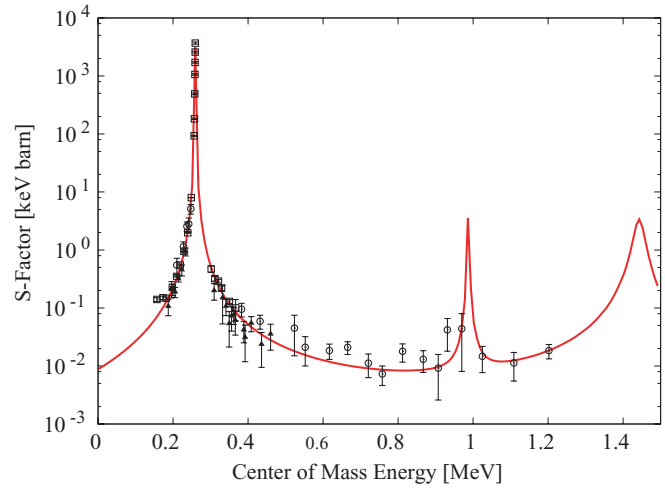

FIG. 12. (Color online) R-matrix analysis of the data for the transition to the 5.18 MeV state. The analysis is based on the experimental data of Refs. [42] (open circles), [40] (open squares), and [39] (solid triangles). The solid line shows the resulting fit and demonstrates the predictive power of the multichannel R-matrix approach in the case of the 1.446 MeV resonance.

and [42] $S_{6.18}(0) = 0.14 \pm 0.05$ keV b. Agreement is also found with the larger value suggested in Ref. [51] of 0.16 ± 0.06 keV b, though the $M1$ background strength was not included as suggested.

The S-factor curve for the 6.79 MeV transition is dominated by external capture, as shown in Fig. 11. The extrapolated $S_{6.79}(0) = 1.30$ keV b is in reasonable agreement with the results of Refs. [40] 1.20 ± 0.05 and [39] 1.15 ± 0.05 keV b. Our results are slightly larger because of our inclusion of the data of Schröder *et al.*; the fits of Refs. [15] and [50], based only on the data of Schröder *et al.*, indeed obtained larger $S(0)$ values, being 1.63 ± 0.17 and 1.40 ± 0.20 keV b, respectively. The systematic underestimation of the Schröder *et al.* data by our calculation indicates the potential value of a remeasurement of this transition at 0.5–2.5 MeV. The fitted ANC of $C_{s3/2} = 4.86$ fm$^{-1/2}$ is in good agreement with those from the previous R-matrix analysis 4.7 ± 0.1 fm$^{-1/2}$ [40] and indirect measurements 4.9 ± 0.5 [50] and 4.6 ± 0.5 [49] fm$^{-1/2}$.

The S-factor curve for the weak transition to the 5.18 MeV state is shown in Fig. 12. The extrapolated S factor $S_{5.18}(0) = 0.01$ keV b, is consistent with the previous result of Ref. [40] of 0.010 ± 0.003 keV b.

The three remaining transitions to the 5.24, 6.86, and 7.28 MeV states, shown in Fig. 13, are dominated by external capture. The extrapolated $S(0) = 0.045$ keV b for the transition to the 6.86 MeV state is in good agreement with the values of 0.03 ± 0.04 [50] and 0.042 ± 0.001 [42] keV b. The subsequent γ decay of the 6.86 and 7.28 MeV states occurs via cascades through the 5.24 MeV state; comparing the sum of these three transitions gives reasonable agreement with the 5.24 to ground state secondary transition data of Refs. [40,42]. The sum of the extrapolated S(0) is $S_{5.24\to0.00}(0) = 0.10$ keV b, in good agreement with the value of 0.070 ± 0.003 from Ref. [40]. The sum of all analyzed transitions shown in Fig. 14 is in excellent agreement with the ^{14}N$(p,\gamma_{\text{total}})$ data of Ref. [45].

The resulting partial widths of the resonance states are shown in Table II, and the ANCs of the bound states in ^{15}O are listed in Table III together with the ANC values determined in previous work. The present ANC values are generally in good agreement with these previous determinations. The extrapolated S-factor values $S(0)$ for the excitation curves of the various primary transitions in this reaction are shown in Table IV, and are in reasonable agreement with previous results, though our total $S(0)$ is somewhat larger than previous determinations.

5. *Summary*

A simultaneous analysis of seven primary transitions for the ^{14}N$(p,\gamma)^{15}$O reaction using a multichannel approach has been presented. The results are best in agreement with those from Ref. [40]. The zero-energy S factor for the ground state transition is larger than that from Ref. [40] attributed to the inclusion of the data from Ref. [39] in our fits. The low-energy extrapolation is very sensitive to data just above the 0.259 MeV resonance. The recent measurements of

TABLE II. Resonance proton and internal γ partial widths for the three strongest transitions.

Energy (MeV)	Γ_p (keV)	$\Gamma_{\gamma_{0.00}}$ (int) (eV)	$\Gamma_{\gamma_{6.18}}$ (int) (meV)	$\Gamma_{\gamma_{6.79}}$ (int) (meV)
−0.504	4.7[a,b]	0.62	–	–
0.259	1.0	0.4×10^{-3}	5.4	9.6
0.985	3.0[a]	0.051	23	–
1.45	32[a]	–	150[a]	–
2.195	250	4.9	–	–
6.00	8000[a]	31	–	–

[a]Parameter fixed in fitting.
[b]ANC (fm$^{-1/2}$).

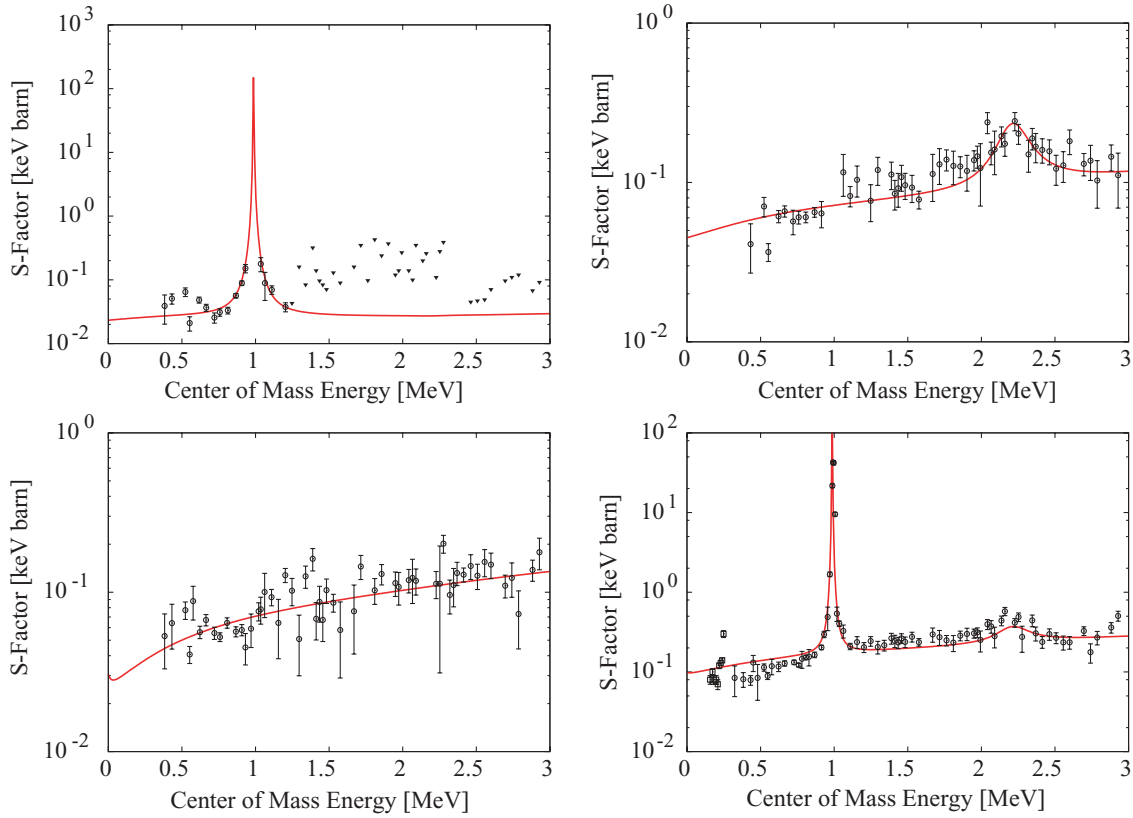

FIG. 13. (Color online) Results from the primary transitions to the 5.24 (top left), 6.86 (top right), and 7.28 (bottom left) MeV state and the sum of these three transitions compared with the secondary data for the ground state transition of the 5.24 MeV state (bottom right). The triangles for the 5.24 MeV primary transition represent experimental upper limits.

Ref. [41], where the data with large summing corrections were neglected, suggest a ground state $S(0)$ of 0.08 keV b lower than the value we obtained, suggesting that further measurements in the range 0.3–1.0 MeV are required. The strong background contributions may be better clarified by data above 2.5 MeV, and the relative strengths of the s and d entrance channel components of the 2.19 MeV resonance would be better determined by including elastic scattering data. This has not been done in the present analysis and will be the subject of a future study taking into account new elastic scattering data.

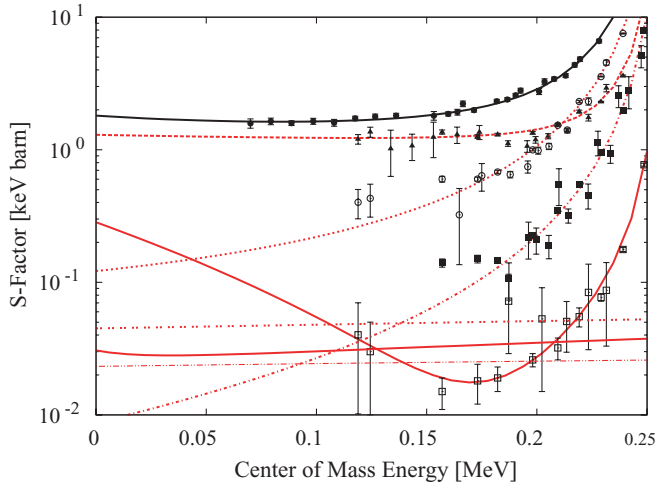

FIG. 14. (Color online) Sum of the R-matrix curves for all primary transitions in the low-energy region (solid black line) in comparison with the total S-factor data for $^{14}\mathrm{N}(p,\gamma_{\mathrm{total}})$ derived in Refs. [44,45] (solid circles).

TABLE III. ANC values $C_{\ell_f I}$ (fm$^{-1/2}$) from the present R-matrix analysis and ANC values from indirect measurements, converted to the present coupling scheme. Note there is a sign ambiguity in the conversion, as the ANCs from transfer measurements are given as $C^2_{\ell_f j}$ only.

Final state	$(\ell_f I)$	AZURE	Ref. [50]	Ref. [49]	Ref. [35]
0.00	$(p,1/2)$	0.23[a]	0.23 ± 0.01	–	1.31[b]
	$(p,3/2)$	7.3[a]	7.3 ± 0.4	–	6.7[b]
6.18	$(p,1/2)$	0.49	0.47 ± 0.03	0.45 ± 0.05	0.49 ± 0.02
	$(p,3/2)$	0.36	0.53 ± 0.03	0.51 ± 0.06	0.54 ± 0.02
6.79	$(s,3/2)$	4.86	4.9 ± 0.5	4.6 ± 0.5	3.74[b]
5.24	$(d,1/2)$	0.54	0.23 ± 0.01	–	0.20 ± 0.02
	$(d,3/2)$	0.21	0.24 ± 0.01	–	0.24 ± 0.02
6.86	$(d,1/2)$	0.46	0.39 ± 0.02	0.41 ± 0.05	0.36 ± 0.03
	$(d,3/2)$	0.48	0.41 ± 0.03	0.44 ± 0.05	0.39 ± 0.04
7.28	$(d,3/2)$	1770	1530 ± 60	1640 ± 180	2300 ± 170

[a]Parameter fixed in fitting.
[b]Error not given.

TABLE IV. Values for the astrophysical S factor resulting from the present (multichannel) and previous R-matrix analyses. Analyzing the ground state transition using the data of Ref. [41] would give an $S(0) \sim 0.08$ keV b lower. Excluding the data of Ref. [42] in the 6.79 MeV transition would give an $S(0) \sim 0.1$ keV b lower.

Energy (MeV)	Astrophysical S factor $S(0)$ (keV b)			
	Present	Ref. [40]	Ref. [39]	Ref. [50]
0.00	0.28	0.25 ± 0.06	0.49 ± 0.08	0.15 ± 0.07
5.18	0.01	0.01 ± 0.003	–	–
5.24[a]	0.10	0.07 ± 0.003	–	0.03 ± 0.04
6.18	0.12	0.08 ± 0.03	0.04 ± 0.01	0.13 ± 0.02
6.79	1.30	1.20 ± 0.05	1.15 ± 0.05	1.40 ± 0.20
Total	1.81	1.61 ± 0.08	1.68 ± 0.09	1.70 ± 0.22

[a]Reference [40] analyzes the secondary transition from the 5.24 MeV decay to the ground state, and Ref. [50] presents results for the transition to the 6.86 MeV state; our value is the sum of the primary transitions to the 5.24, 6.86, and 7.28 MeV states.

The fit for the transition to the 6.18 MeV state gives a larger $S(0)$ than in Ref. [40] because of our inclusion of a $I = 3/2$ external capture component. The extrapolated S factor for the dominant transition to the 6.79 MeV state is larger than the previous analysis [40] because of our inclusion of the data of Ref. [42], the normalization of which should be checked with new measurements in the 0.5–2.5 MeV region. Our analysis of the weakly contributing transitions is in good agreement with previous determinations.

The sum of all fits for primary transitions at low energies is marginally larger than previous estimates but is in excellent agreement with $(p,\gamma_{\text{total}})$ data of Refs. [44,45]. There is still considerable uncertainty in the ground state transition, which is not distinguished by the $(p,\gamma_{\text{total}})$ data, despite extending as low as 70 keV.

C. ^{16}O$(p,\gamma)^{17}$F reaction

The ^{16}O$(p,\gamma)^{17}$F reaction triggers the second CNO cycle or NO cycle [19]. It is initiated primarily on the ^{16}O seed abundance in stellar material which may be slightly enhanced by leakage from the CN cycle through the ^{15}N$(p,\gamma)^{16}$O reaction. Because of the low cross section, the reaction is the slowest one in the NO cycle and determines its energy contribution to the overall CNO burning. The reaction is dominated by direct capture components to the ground state ($J^\pi = 5/2^+$) and the first excited state ($J^\pi = 1/2^+$) in ^{17}F, and is considered to be one of the standard cases for a pure direct capture mechanism [4,5]. As such, this example is used to demonstrate the full inclusion of the external capture component in the AZURE code.

1. *R-matrix analysis*

The R-matrix analysis was performed using the data of Ref. [54], corrected for summing effects in Ref. [55]. The experimental errors have been augmented [55] to include an additional 10%, which was added in quadrature with the original errors of Ref. [54]. A systematic error of 10% has been identified in Appendix B of Ref. [56]. It is not clear if this is the 10% error referred to in Ref. [55]. The data covers an energy range from 0.23 to 3.75 MeV in the laboratory frame. Two resonances appear in the yield curve, at $E_p = 2.659$ MeV ($J^\pi = 1/2^-$) and $E_p = 3.463$ MeV ($J^\pi = 5/2^-$), and were included in the present analysis. Because of their small total widths, these resonances have only a localized effect on the yield curve. A $J^\pi = 3/2^-$ background pole was also included in the analysis. An external capture contribution to both bound states was also considered, with the assumption that the ground state and first excited state could be described by a valance proton occupying $1d_{5/2}$ and $1s_{1/2}$ orbitals, respectively. Only $E1$ contributions to external capture were included in the analysis, proceeding through $l_i = 1$ ($J^\pi = 1/2^-, 3/2^-$) and $l_i = 3$ ($J^\pi = 5/2^-, 7/2^-$) partial waves. A channel radius of $a_c = 5.0$ fm was used in the present calculation, adopted from Ref. [55]. The resulting AZURE fits can be seen in Figs. 15 and 16. In both figures, the components arising from internal R-matrix capture, hard-sphere external capture (EC), and resonant external capture (ERC) are explicitly shown. The background pole contributes very little to the internal contribution, but it is significant in the ERC component. This is, in effect, compensating for an additionally needed scattering phase shift in the external capture beyond the hard-sphere approximation.

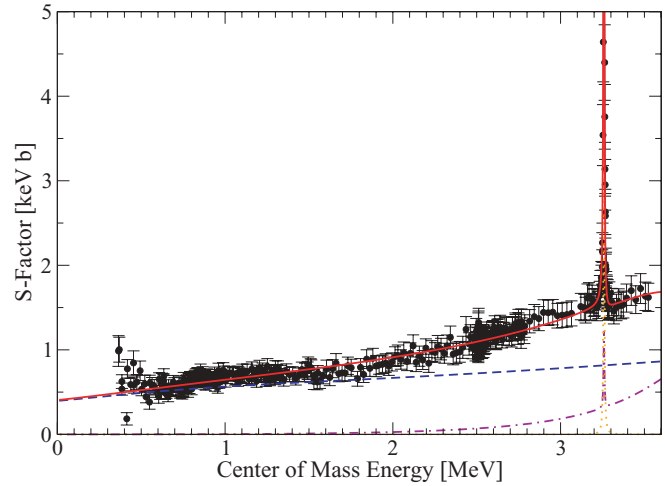

FIG. 15. (Color online) AZURE fit of the ^{16}O$(p,\gamma_0)^{17}$F reaction. The red (solid) line indicates the AZURE best fit. The blue (dashed) line is the hard-sphere external capture (EC) component, while the violet (dash-dot) line is the resonant external capture (ERC) contribution. The orange (dotted) line is the negligible internal R-matrix contribution.

2. *Reaction parameters and astrophysical S factor*

At astrophysical energies, the cross section is almost entirely determined by the hard-sphere external capture component (EC), which is scaled by the asymptotic normalization coefficient (ANC) of the bound state of interest. For the ground state transition, the present analysis yields an ANC of $C = 1.05$ fm$^{-1/2}$, and for the first excited state $C = 80.7$ fm$^{-1/2}$. Morlock *et al.* [54] quote an effective gas target thickness on the order of the total width of the two resonances present in the yield curve. Corrections for target effects were not included in the present analysis, as the resonances contribute negligibly

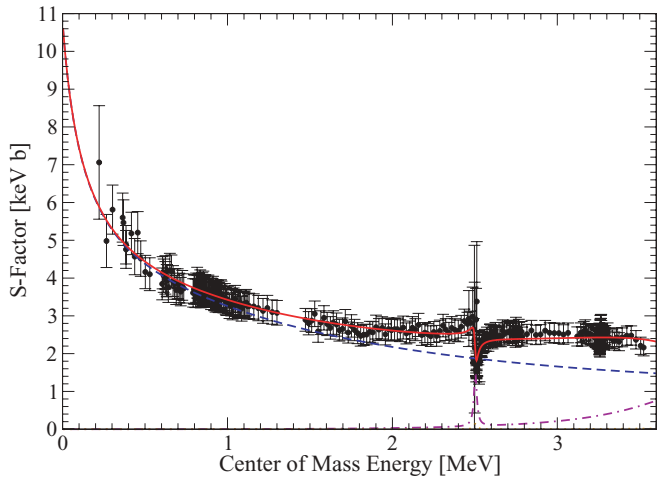

FIG. 16. (Color online) Same as Fig. 15, but for the $^{16}O(p,\gamma_1)^{17}F$ reaction.

to the reaction rate away from their local energies, and therefore physical widths are not quoted here. The R-matrix fit parameters, including the fitted background state, are given in Table V. The present analysis yields a total astrophysical S factor of $S(90\,\text{keV}) = 8.07\,\text{keV b}$.

3. *Comparison with previous work*

Iliadis *et al.* [55] quote an ANC of $C = 1.13 \pm 0.01\ \text{fm}^{-1/2}$ for the ground state, and $C = 82.3 \pm 0.3\ \text{fm}^{-1/2}$ for the first excited state. The present values differ from those values by 7% and 2% for the ground and first excited states, respectively. These differences may arise from an alternative treatment of the nonresonant components in the internal R matrix. Regardless of these discrepancies, the present S factor at 90 keV is in good agreement with the extrapolation illustrated in Fig. 8 of Ref. [55]. Gagliardi *et al.* [57] have indirectly measured the ANCs for the ground and first excited state as a test case for the determination of low-energy capture S factors via transfer reactions. They obtain $C = 1.04 \pm 0.05\ \text{fm}^{-1/2}$ for the ground state and $C = 80.6 \pm 4.2\ \text{fm}^{-1/2}$ for the first excited state. The ANCs obtained in the current analysis are in excellent agreement with these indirect values.

V. SUMMARY

This study presents a new R-matrix code, AZURE, which has been designed specifically for the nuclear astrophysics community. AZURE is particularly useful in the analysis of low-energy charged-particle induced reactions. Resonant and nonresonant direct contributions have been included within a full multilevel multichannel framework, allowing for reliable extrapolations to astrophysically relevant energy regions. Several examples of the capabilities of AZURE have been given above in the context of stellar hydrogen burning, demonstrating the usefulness of the program in evaluating cross sections of interest to the field of nuclear astrophysics. The examples presented here, $^{12}C(p,\gamma)^{13}N$, $^{14}N(p,\gamma)^{15}O$, and $^{16}O(p,\gamma)^{17}F$, are significant to the understanding of stellar hydrogen burning through the CNO cycles in our sun and in massive stars. The reliability of the extrapolation of the existing low-energy data has been a matter of intense debate over the last decade. The use of R-matrix theory has added considerably to our understanding and interpretation of the low-energy cross sections of these and other reactions. Multichannel R-matrix analysis offers the possibility of reducing the uncertainties in this extrapolation and interpretation of low-energy reaction data via the additional constraint provided by the simultaneous treatment of multiple reaction channels.

Extensive careful analysis of all the chosen examples has been performed in the past. The present analysis shows excellent agreement with these previous studies which demonstrates the reliability of AZURE. Beyond this, the multichannel analysis feature of AZURE added significantly to the reduction of the uncertainty in the extrapolation by introducing new constraints for the reaction parameters.

The selected examples were radiative capture reactions where AZURE has been used to explore in detail the various reaction components in the low-energy range. Adding the elastic scattering channel into the fit proved to be beneficial for providing constraints to the ground state ANC which defines the strength of the external capture channel in the $^{12}C(p,\gamma)^{13}N$ cross section. The multichannel approach was particularly useful in the analysis of $^{14}N(p,\gamma)^{15}O$, where the seven radiative capture channels were fitted parallel. This certainly generates a more consistent parameter set for resonant and external capture components than the usual approach of fitting each channel separately. The $^{16}O(p,\gamma)^{17}F$ example demonstrated the capability of AZURE to fit reactions dominated by external capture components.

While the present paper focuses exclusively on the low-energy fit of radiative capture reactions, AZURE also provides the possibility for the parallel fitting of particle channels. This will be demonstrated in a number of upcoming papers where new experimental data will be used to present an R-matrix analysis to the critical CNO reaction branches $^{15}N(p,\gamma)^{16}O$-$^{15}N(p,\alpha)^{12}C$ and $^{17}O(p,\gamma)^{18}F$-$^{17}O(p,\alpha)^{14}N$.

TABLE V. Physical R-matrix fit parameters for the $^{16}O(p,\gamma)^{17}F$ reaction.

E_λ (keV)	E_p (keV)	γ_p (MeV$^{-1/2}$)	γ_{γ_0} (int) (MeV$^{-1/2}$)	γ_{γ_1} (int) (MeV$^{-1/2}$)
0.00	−638	$C_{d_{5/2}} = 1.05\ \text{fm}^{-1/2}$	–	–
495	−112	$C_{s_{1/2}} = 80.7\ \text{fm}^{-1/2}$	–	–
3103	2659	0.1415	–	0.04359
3859	3463	0.2456	0.05344	–
4711	4368	0.7519	−0.09586	0.00404

ACKNOWLEDGMENTS

This work has been supported extensively by the Joint Institute for Nuclear Astrophysics (JINA) under NSF Grant PHY0216783. R.E.A. thanks the Natural Sciences and Engineering Research Council of Canada for support through the DRAGON rant at TRIUMF. E.C.S. is grateful for support from the UK Science and Technologies Funding Council through Grant EP/D003628. The work of C.R.B. was supported by the US Department of Energy, through Grant Nos. DE-FG52-06NA26187 and DE-FG02-88ER40387. In addition, the authors are particular indebted to Fred C. Barker (ANU, Canberra, Australia) and Erich Vogt (TRIUMF, Vancouver, Canada) for many discussions and their help in the AZURE *R*-matrix project. The authors are grateful to H.-P. Trautvetter for providing information about the analysis of ^{14}N$(p,\gamma)^{15}$O data and for testing pilot versions of the AZURE code. The authors finally want to thank Gianluca Imbriani (Universitá Federico II, Naples, Italy) for helpful and critical remarks about the analysis presented here.

[1] C. Angulo *et al.*, Nucl. Phys. A **656**, 3 (1999).
[2] W. A. Fowler, G. R. Caughlan, and B. A. Zimmerman, Annu. Rev. Astron. Astrophys. **5**, 525 (1967).
[3] H. Gove, in *Nuclear Reactions*, edited by P. Endt and M. Demeur (North-Holland, Amsterdam, 1959), Vol. I, Chap. VI, p. 259.
[4] R. Christy and I. Duck, Nucl. Phys. **24**, 89 (1961).
[5] C. Rolfs, Nucl. Phys. A **217**, 29 (1973).
[6] C. Rolfs and R. Azuma, Nucl. Phys. A **227**, 291 (1974).
[7] M. Wiescher *et al.*, Nucl. Phys. A **349**, 165 (1980).
[8] D. Sargood, Phys. Rep. **93**, 61 (1982).
[9] A. Aprahamian, K. Langanke, and M. Wiescher, Prog. Part. Nucl. Phys. **54**, 535 (2005).
[10] E. Wigner, Phys. Rev. **70**, 15 (1946).
[11] E. Wigner, Phys. Rev. **70**, 606 (1946).
[12] E. P. Wigner and L. Eisenbud, Phys. Rev. **72**, 29 (1947).
[13] W. E. Kieser, R. E. Azuma, and K. P. Jackson, Nucl. Phys. A **331**, 155 (1979).
[14] F. C. Barker and T. Kajino, Aust. J. Phys. **44**, 369 (1991).
[15] C. Angulo and P. Descouvemont, Nucl. Phys. A **690**, 755 (2001).
[16] E. Adelberger *et al.*, Rev. Mod. Phys. **70**, 1265 (1998).
[17] F. C. Barker, Aust. J. Phys. **25**, 341 (1972).
[18] C. R. Brune, Phys. Rev. C **66**, 044611 (2002).
[19] G. Caughlan and W. Fowler, Astrophys. J. **136**, 453 (1962).
[20] G. Caughlan and W. Fowler, Astron. J. **70**, 670 (1965).
[21] A. Lane and R. Thomas, Rev. Mod. Phys. **30**, 257 (1958).
[22] E. Vogt, Rev. Mod. Phys. **34**, 723 (1962).
[23] C. Ugalde, Ph.D. thesis, University of Notre Dame, 2005.
[24] A. Lane and J. Lynn, Nucl. Phys. **17**, 563 (1960).
[25] R. J. Holt, H. E. Jackson, R. M. Laszewski, J. E. Monahan, and J. R. Specht, Phys. Rev. C **18**, 1962 (1978).
[26] R. G. Seyler and H. R. Weller, Phys. Rev. C **20**, 453 (1979).
[27] F. James, *Minuit: Function Minimization and Error Analysis*, 94.1 ed. (CERN, Geneva, Switzerland, 1994).
[28] E. Anderson *et al.*, LAPACK *User's Guide*, 3rd ed. (Society for Industrial and Applied Mathematics, Philadelphia, 1999).
[29] J. Vogl, Ph.D. thesis, California Institute of Technology, 1963.
[30] F. C. Barker and N. Ferdous, Aust. J. Phys. **33**, 691 (1980).
[31] H. Meyer, G. Plattner, and I. Sick, Z. Phys. A **279**, 41 (1976).
[32] V. A. Poyarkov and I. V. Sizov, Yad. Fiz. **45**, 1515 (1987).
[33] A. Z. Kiss, E. Koltay, and E. Somorjai, Acta Phys. Hung. **65**, 277 (1989).
[34] F. Ajzenberg-Selove, Nucl. Phys. A **523**, 1 (1991).
[35] S. V. Artemov, E. A. Zaparov, and G. K. Nie, Bull. Russ. Acad. Sci. **67**, 1741 (2003).
[36] S. Degl'Inocenti, G. Fiorentini, B. Ricci, and F. L. Villante, Phys. Lett. B **590**, 13 (2004).
[37] W. Haxton and A. Serenelli, Astrophys. J. **687**, 678 (2008).
[38] A. Formicola *et al.*, Phys. Lett. B **591**, 61 (2004).
[39] R. C. Runkle, A. E. Champagne, C. Angulo, C. Fox, C. Iliadis, R. Longland, and J. Pollanen, Phys. Rev. Lett. **94**, 082503 (2005).
[40] G. Imbriani *et al.*, Eur. Phys. J. A **25**, 455 (2005).
[41] M. Marta *et al.* (LUNA Collaboration), Phys. Rev. C **78**, 022802(R) (2008).
[42] U. Schröder *et al.*, Nucl. Phys. A **467**, 240 (1987).
[43] H.-P. Trautvetter (personal communication).
[44] A. Lemut *et al.*, Phys. Lett. B **634**, 483 (2006).
[45] D. Bemmerer *et al.*, Nucl. Phys. A **779**, 297 (2006).
[46] P. F. Bertone, A. E. Champagne, D. C. Powell, C. Iliadis, S. E. Hale, and V. Y. Hansper, Phys. Rev. Lett. **87**, 152501 (2001).
[47] D. Schürmann, R. Kunz, I. Lingner, C. Rolfs, F. Schümann, F. Strieder, and H.-P. Trautvetter, Phys. Rev. C **77**, 055803 (2008).
[48] K. Yamada *et al.*, Phys. Lett. B **579**, 265 (2004).
[49] P. F. Bertone, A. E. Champagne, M. Boswell, C. Iliadis, S. E. Hale, V. Y. Hansper, and D. C. Powell, Phys. Rev. C **66**, 055804 (2002).
[50] A. M. Mukhamedzhanov *et al.*, Phys. Rev. C **67**, 065804 (2003).
[51] S. O. Nelson, M. W. Ahmed, B. A. Perdue, K. Sabourov, A. L. Sabourov, A. P. Tonchev, R. M. Prior, M. Spraker, and H. R. Weller, Phys. Rev. C **68**, 065804 (2003).
[52] M. Lambert and M. Durand, Phys. Lett. B **24**, 287 (1967).
[53] A. Gurbich, Nucl. Instrum. Methods Phys. Res. B **266**, 1193 (2008).
[54] R. Morlock, R. Kunz, A. Mayer, M. Jaeger, A. Müller, J. W. Hammer, P. Mohr, H. Oberhummer, G. Staudt, and V. Kölle, Phys. Rev. Lett. **79**, 3837 (1997).
[55] C. Iliadis, C. Angulo, P. Descouvemont, M. Lugaro, and P. Mohr, Phys. Rev. C **77**, 045802 (2008).
[56] R. Morlock, Ph.D. thesis, Universität Stuttgart, 1997.
[57] C. Gagliardi *et al.*, Phys. Rev. C **59**, 1149 (1999).